Fermi National Accelerator Laboratory

FERMILAB-TM-2001

Crossing Angle Induced Dispersion in LHC

F. Méot

Fermi National Accelerator Laboratory
P.O. Box 500, Batavia, Illinois 60510

July 1997

Operated by Universities Research Association Inc. under Contract No. DE-AC02-76CH03000 with the United States Department of Energy

Disclaimer

This report was prepared as an account of work sponsored by an agency of the United States Government. Neither the United States Government nor any agency thereof, nor any of their employees, makes any warranty, expressed or implied, or assumes any legal liability or responsibility for the accuracy, completeness, or usefulness of any information, apparatus, product, or process disclosed, or represents that its use would not infringe privately owned rights. Reference herein to any specific commercial product, process, or service by trade name, trademark, manufacturer, or otherwise, does not necessarily constitute or imply its endorsement, recommendation, or favoring by the United States Government or any agency thereof. The views and opinions of authors expressed herein do not necessarily state or reflect those of the United States Government or any agency thereof.

Distribution

Approved for public release; further dissemination unlimited.

Crossing Angle Induced Dispersion In LHC

F. Méot *
Fermi National Accelerator Laboratory
P.O. Box 500, Batavia, Illinois 60510

Report FERMILAB-TM-2001

July 1, 1997

Abstract

Beam crossing and separation schemes in the LHC interaction regions impose non-zero horizontal and vertical closed orbits in the low-β triplets. This induces dispersive terms in the equation of motion, of first order in momentum deviation. The related perturbative periodic dispersion is derived ; propagation, multiple-crossing interference, perturbative effects around the LHC ring are investigated and quantified. It is shown that they are large enough that local correction be justified. Compensation schemes are presented, possibly compatible with the recently designed modular IR optics.

*On leave from CEA/DSM-Saclay, France

Contents

1 Introduction **3**

2 Anomalous dispersion due to beam crossing/off-centering geometry at IP **3**
2.1 Equation of the anomalous dispersion 3
2.2 Upper limits of the perturbation 5
2.3 Comparison with the effects of the separator/recombiner optics 6

3 Typical effects of crossing angle geometry **7**
3.1 Crossing at a single IP 7
3.2 Interferences 8

4 Survey of the perturbative effects around the ring **10**
4.1 Perturbative closed dispersion around LHC 10
4.2 Beam size related effects 11

5 Correction schemes **12**
5.1 Self-absorption within regular IR tuning procedures 12
5.2 Quadrupole correction of the horizontal dispersion 13
5.3 Partial compensation from interference 16
5.4 Correction of the vertical dispersion with skew quadrupoles 17

A Appendix : Beam crossing and off-centering schemes **37**

B Appendix : Sums related to the elementary kick model **37**

C Appendix : Simplified expressions for the anomalous dispersion **39**

D Appendix : MAD simulations **41**
D.1 Single x-crossing/z-off-centering at $IP5$. Optical parameters in the vicinity of the IP's 41
D.2 Multiple crossing, at $IP1, 2, 5$ and 8. Optical parameters in the vicinity of the IP's . 42

E Appendix : MAD match file **43**

1 Introduction

Crossing angle and orbit off-centering schemes at beam-beam interaction points (IP) in the LHC ring are foreseen [1]-[3], for the purpose of full separation of the beams during the injection phase, or early separation of the beams beyond the IP during collision, in order to reduce as much as possible harmful effects related to beam-beam interactions in that region where they share a common vacuum pipe. Both planes may be affected by crossing or off-centering, e.g., in the 45 deg. inclined crossing plane scheme. From the orbit design viewpoint, this means non-zero closed orbit angle (crossing) or non-zero closed orbit off-centering (separation) at the IP of concern. The orbit bump can be canceled by pairs of dipoles placed beyond the separator/recombiner magnets D1-Left and D1-right since from thereon the two proton beams are in separate pipes.

Such orbit geometry imposes horizontal and vertical off-centerings in the low-β triplets, which has sensible effect on dispersion in collision optics when betatron functions reach very large values. In terms of the equations of motion, the non-zero closed orbit (c.o.) induces dispersive terms of first order in momentum deviation, with so-called anomalous dispersion as the closed solution.

The purpose of the present study is two-fold. On the one hand, study in detail and provide an understanding of the building-up and effects of the anomalous dispersion ; on the other hand investigate possible compensation schemes, assimilable within the existing interaction region (IR) optical assembly. Numerical applications and simulations undertaken in the report are based on the Version 4.2 of the LHC optics [1], while LHC Version 5 optics was not yet stabilized at the time this study was carried out ; however they differ mostly by an additional quadrupole in the outer triplet, which should not change anything fundamental as to analysis or correction of anomalous dispersion. MAD simulations are performed wherever necessary [4], with the regular LHC lattice files [5]. A typical c.o. geometry has been designed for this study ; it is inspired from general descriptions already available [2][3], apart from some non-fundamental specifities clearly pointed out. Details are given in Appendix A.

The report is organized as follows. In section 2 the equation of motion is established and an expression for the anomalous dispersion is worked out in the elementary kick model ; $\pm 10^{-4} rad$ c.o. angle is shown to have non-negligible effect, while $\pm 10^{-3} m$ off-centering is less harmful. In section 3 simplified expressions relevant with LHC optics are derived which allow accurate quantifying of the perturbative effects under c.o. angle ; interference effects due to multiple crossing are also investigated and quantified. Section 4 gives detailed survey and plots of the anomalous dispersion around LHC. Section 5 presents correction schemes, assimilable as part of the regular up-to-date IR optics.

2 Anomalous dispersion due to beam crossing/off-centering geometry at IP

2.1 Equation of the anomalous dispersion

Dispersive effects related to c.o. geometry can be derived from the equation of motion of an off-momentum particle. Up to the second order in transverse excursion y(s) (y stands for x or z, s is the azimuth) with respect to the machine reference axis (hence the subscript r) and momentum deviation δ the equation writes [6]

$$d^2 y_r/ds^2 + K(s) y_r = (1-\delta)\Delta B(s)/B\rho + \delta/\rho(s) + K(s) y_r \delta \tag{1}$$

where $B\rho$ is the particle rigidity, K(s) is the quadrupole strength, $1/\rho$(s) the curvature (identically zero if y=z) and δ is the momentum deviation. The field defect term $\Delta B(s)/B\rho$ is introduced by the c.o. bump dipoles (it stands for $-\Delta B_z(s)/B\rho$ if y=x, $\Delta B_x(s)/B\rho$ if y=z) and the coefficient $(1-\delta)$ accounts for their first order chromatic effect. The term $K(s) y_r \delta$ is second order dispersive

effect introduced by the quadrupoles. The equation of motion with respect to the c.o. is obtained by introducing $y_r = y_{co} + y$. Considering that the c.o. is solution of

$$d^2 y_{co}/ds^2 + K(s) y_{co} = \Delta B(s)/B\rho \tag{2}$$

and dropping the second order term $K(s)y\delta$ this gives to first order in y and δ

$$d^2 y/ds^2 + K(s) y = [-\Delta B(s)/B\rho + 1/\rho(s) + K(s) y_{co}]\delta \tag{3}$$

This equation shows that the c.o. bump is at the origin of anomalous first order dispersion $d_y = y/\delta$ whose source term $K(s)y_{co}\delta$ takes its origin in the low-β quadrupoles and any other quadrupole contained within the limits of the bump. It also shows that the horizontal anomalous dispersion superposes on the regular first order dispersion $d_x(s)$ of source term $1/\rho(s)$ (the main dipoles). We are therefore concerned with the particular, closed solution of

$$d^2 d_y/ds^2 + K(s) d_y = -\Delta B(s)/B\rho + K(s) y_{co} \tag{4}$$

which in the case of the horizontal motion ($y \equiv x$) adds to the first order dispersion $d_x(s)$, and in the case of the vertical motion is free standing periodic dispersion. The solution for the sole driving term $-\Delta B(s)/B\rho$ is that of Eq. (2) with opposite sign, i.e., $-y_{co}(s)$. Therefore the equation to solve reduces to

$$d^2 d_y/ds^2 + K(s) d_y = K(s) y_{co} \tag{5}$$

while keeping in mind that its solution d_y is to be subtracted the c.o. $y_{co}(s)$ everywhere this last is non-zero. Eq. (5) can be solved in the elementary kick approximation $K(s)y_{co}(s) = \int K(s)y_{co}(s)\delta(s-s_q)ds_q$ [$\delta(s-s_q)$ is the Dirac impulse at kick azimuth s_q]. Integration of Eq. (2.5) provides the elementary kick amounts

$$\Delta(dd_y/ds) = \int K(s) y_{co}(s)\delta(s-s_q)ds = (KL)_q y_{co}(s_q) \tag{6}$$

Comparison can be performed with the kick produced by a separator/recombiner dipole : D1 strength is about $2.17\,10^{-3} rad$ while numerical calculation with $y'^* = 10^{-4} rad$ c.o. angle gives, for odd-IR low-β triplet, $\sum (KL)_q y_{co}(s_q) \approx 0.125\,10^{-3} rad$ i.e., about 20 times less (note that, with such angle at IP the c.o. reaches $4.7\,10^{-3} m$ in the quadrupoles). However comparison of the respective effects on dispersion needs deeper insight (section 2.3). Eq. (2.5) now writes

$$d^2 d_y/ds^2 + K(s) d_y = \int K(s) y_{co}(s)\delta(s-s_q)ds_q \tag{7}$$

and can be solved by classical methods [7]. This leads to the perturbative closed dispersion solution of Eq. (4), and its derivative

$$\begin{aligned}
d_y(s) &= -y_{co}(s) + \sqrt{\beta(s)}/(2\sin\pi\nu)\sum (KL)_q y_{co}(s_q)\sqrt{\beta(s_q)}\cos\nu[\pi - |\phi(s)-\phi(s_q)|] \\
d'_y(s) &= 1/[2\sin\pi\nu\sqrt{\beta(s)}]\sum (KL)_q y_{co}(s_q)\sqrt{\beta(s_q)}\{-\alpha(s)\cos\nu[\pi - |\phi(s)-\phi(s_q)|] \\
&\quad +\epsilon\sin\nu[\pi - |\phi(s)-\phi(s_q)|]\} \\
&\quad [\epsilon = \pm 1\, for\ resp.\ \phi(s) \gtrless \phi(s_q), \forall q]
\end{aligned} \tag{8}$$

where $\phi(s) = 1/\nu \int ds/\beta$ is the normalized betatron phase (the integral extends from arbitrary zero to current azimuth s), $\phi(s_q)$ = normalized phase at the kick, β = betatron function, ν = machine tune, $y_{co}(s_q)$ = closed orbit at the kick. Note that a reasonable fractioning of the low-β quadrupoles takes care of possibly strong variations of the betatron function in the triplets. The discrete summation $\sum$

extends over those quadrupoles situated within the local c.o. bump responsible for beam separation and/or crossing. In case several bumps are settled at various IP's along the machine, a convenient way to calculate the overall perturbation is to solve Eq. (4) for each bump, and sum the individual solutions $d_y(s)$ (Eq. 8).

It is not uninteresting to verify that solutions analogous to Eq. (8) arise in the treatment of gamma transition jump [8], which is also concerned with dispersion perturbation, induced by non-zero chromatic closed orbit in quadrupole families [9].

Assuming that all c.o. dipoles are situated beyond the quadrupoles sources of the anomalous dispersion, it is leisurable to introduce the c.o. in terms of the unperturbed first order optics by its transport from the IP,

$$y_{co}(s_q) = y^* \sqrt{[\beta(s_q)/\beta^*}\cos\nu[\phi(s_q)-\phi^*] + y'^* \sqrt{\beta(s_q)\beta^*}\sin\nu[\phi(s_q)-\phi^*] \tag{9}$$

in which the subscript * denotes quantities taken at the IP, y^* is the c.o. off-centering (half beam-beam separation at IP), y'^* is the c.o. angle (half crossing angle), and beam divergence $\alpha^* = 0$ is assumed. Reporting Eq. (9) in Eq. (8) yields

$$\begin{aligned} d_y(s) &= -y_{co}(s) \\ &+ y^* \sqrt{\beta(s)/\beta^*}/(2\sin\pi\nu)\sum(KL)_q\beta(s_q)\cos\nu[\phi(s_q)-\phi^*]\cos\nu[\pi-|\phi(s)-\phi(s_q)|] \\ &+ y'^* \sqrt{\beta(s)\beta^*}/(2\sin\pi\nu)\sum(KL)_q\beta(s_q)\sin\nu[\phi(s_q)-\phi^*]\cos\nu[\pi-|\phi(s)-\phi(s_q)|] \end{aligned} \tag{10}$$

2.2 Upper limits of the perturbation

Beyond the low-β triplets associated with the non-zero c.o. Eq. (8) can be written under the form

$$d_y(s)/\sqrt{\beta(s)} = -y_{co}(s)/\sqrt{\beta(s)} + \bar{D}_y\cos\nu[\phi(s)+\Omega] \tag{11}$$

with the peak amplitude

$$\begin{aligned} \bar{D}_y &= \{\,[\sum(KL)_q y_{co}(s_q)\sqrt{\beta(s_q)}\cos\nu(\pi+\epsilon\phi(s_q))]^2 \\ &+ [\sum(KL)_q y_{co}(s_q)\sqrt{\beta(s_q)}\sin\nu(\pi+\epsilon\phi(s_q))]^2\,\}^{1/2}/(2\sin\pi\nu) \\ &\quad [\epsilon = \pm 1\ for\ resp.\ \phi(s) \gtrless \phi(s_q), \forall q] \end{aligned} \tag{12}$$

attained at normalized betatron phase Ω such that

$$\begin{aligned} \tan(\Omega\nu) &= [\sum(KL)_q y_{co}(s_q)\sqrt{\beta(s_q)}\sin\nu(\pi+\epsilon\phi(s_q))] \\ &/ [\sum(KL)_q y_{co}(s_q)\sqrt{\beta(s_q)}\cos\nu(\pi+\epsilon\phi(s_q))] \end{aligned} \tag{13}$$

Calculation of the cosine and sine sums for $\phi(s)\gtrless\phi(s_q)$ (App. B) from the first order optical functions in collision optics yields

$$\bar{D}_x|_{x^*=0} \approx 170\,x'^*,\ \bar{D}_z|_{z^*=0} \approx 158\,z'^*,\ \bar{D}_x|_{x'^*=0}/x^* \approx \bar{D}_z|_{z'^*=0}/z^* \approx 2 \tag{14}$$

Considering that β_x and β_z have similar shapes Eq. (14) shows that the perturbation due to $10^{-4}rad$ c.o. angle is about 8 times that due to $10^{-3}m$ c.o. off-centering at IP. Typical upper limits to $d_y(s) = \bar{D}_y\sqrt{\beta(s)}$ are, 0.23 m in the arcs ($\beta_{max} = 178\,m/rad$) ; 1.13 m in the odd-type low-β triplets ($\beta_{max} = 4430m/rad$) ; 1.07 m in the even-type low-β triplets ($\beta_{max} = 4020\,m/rad$). These extrema are attained *iff* adequate betatron phase is reached at β_{max}. However this shows that the survey of anomalous dispersion and possibly its compensation deserve finer insight.

2.3 Comparison with the effects of the separator/recombiner optics

It is not uninteresting to compare the dispersive effects due to the non-zero c.o. at IP to those induced by the separator/recombiner dipoles D1/D2, in particular in view of possible simultaneous compensation of both by a common optical assembly such as proposed in Ref.[10]. One single separator dipole (D1 or D2) with bend angle Θ_D excites a closed dispersion of the form

$$^{D}d_x(s)/\sqrt{\beta(s)} = \Theta_D/(2\sin\pi\nu) < \sqrt{\beta(s_D)} > \cos\nu[\pi - |\phi(s) - \phi(s_D)|] \tag{15}$$

where $< \sqrt{\beta(s_D)} >$ denotes the mean value of $\sqrt{\beta(s_D)}$ over the dipole, and the normalized betatron phase $\phi(s_D)$ is supposed constant over a dipole. The perturbation beyond D1/D2 range and in particular in the arcs is obtained by taking $\phi(s) > \phi(s_{D1}), \phi(s_{D2})$ [$\phi(s) < \phi(s_{D1}), \phi(s_{D2})$ would do as well ; the former has the merit of eliminating the absolute value in the cosine argument] and superimposing the effects of D1 and D2, which gives the closed solution

$$\begin{aligned} ^{D1/D2}d_x(s) \quad / \quad & \sqrt{\beta(s)} = \Theta_D/(2\sin\pi\nu)\{ < \sqrt{\beta(s_{D1})} > \cos\nu[\pi \\ - \quad & |\phi(s) - \phi(s_{D1})|] - < \sqrt{\beta(s_{D2})} > \cos\nu[\pi - |\phi(s) - \phi(s_{D2})|] \} \end{aligned} \tag{16}$$

This expression can be written under the form

$$^{D1/D2}d_x(s)/\sqrt{\beta(s)} = ^{D1/D2}\bar{D}_x \cos\nu[\phi(s) + \tau] \tag{17}$$

It can be assumed that $\phi(s_{D1}) \approx \phi(s_{D2})$ (this is true at about $2\pi\, 10^{-3}$ in collision optics), which leads to

$$^{D1/D2}\bar{D}_x \approx \Theta_D/(2\sin\pi\nu)[< \sqrt{\beta(s_{D1})} > - < \sqrt{\beta(s_{D2})} >] \tag{18}$$

The peak amplitude $^{D1/D2}\bar{D}_x$ can be evaluated by taking $\Theta_D = 2.17\, 10^{-3} rad$ and $< \sqrt{\beta(s_{D1})} > \approx \sqrt{< \beta(s_{D1}) >}$, which gives

$$\begin{aligned} ^{D1/D2}\bar{D}_x|_{Left} \quad & \approx \quad 2.17\, 10^{-3}/(2\sin 63.28\pi)(\sqrt{4000} - \sqrt{2100}) \approx 250\, 10^{-4} m \\ ^{D1/D2}\bar{D}_x|_{Right} \quad & \approx \quad 2.17\, 10^{-3}/(2\sin 63.28\pi)(\sqrt{4000} - \sqrt{2100}) \approx -210\, 10^{-4} m \end{aligned} \tag{19}$$

The overall effect of the π/ν apart left and right separator dipole pairs is obtained by summing these two values, namely

$$^{D1/D2}\bar{D}_x|_{Left+Right} \approx 460\, 10^{-4} \tag{20}$$

Given $\beta_x \approx 180\, m$ this yields the modulation $^{D1/D2}\bar{D}_x|_{Left+Right}\sqrt{\beta_x} \approx \pm 0.6\, m$. This can readily be compared to the analogous coefficients in presence of $10^{-4} rad$ c.o. angle (Eq. 14), namely

$$^{Crossing}\bar{D}_x \;/\; ^{D1/D2}\bar{D}_x \approx 170/460 \approx 35\% \tag{21}$$

In other words, the extremum of the modulation in the arcs due to $10^{-4} rad$ c.o. angle at IP can be expected to amount to $\pm 0.35 \times 0.6\, m \approx \pm 0.2\, m$. It also means that a correction scheme intended to compensate the dispersion introduced by the separator/recombiner optics must have its strength changed (increased or decreased depending on the sign of the crossing) by about 35% so as to take care additionally of $\pm 10^{-4} rad$ c.o. angle effects (see Fig. 10).

3 Typical effects of crossing angle geometry

In the following we investigate and quantify the major effects of the non-zero c.o. in the low-β triplets, in terms of the extrema and other characteristic values of the perturbative dispersion so induced around the ring. We consider for simplification the sole crossing scheme ($y^* = 0, y'^* \neq 0$), which has the major perturbative effect as shown above. As a consequence we are concerned with (Eq. 10)

$$\begin{aligned} d_y(s) &= -y_{co}(s) \\ &+ y'^* \sqrt{\beta(s)\beta^*}/(2\sin\pi\nu) \sum (KL)_q \beta(s_q) \sin\nu[\phi(s_q) - \phi^*] \cos\nu[\pi - |\phi(s) - \phi(s_q)|] \end{aligned} \tag{22}$$

which, we recall, is valid as long as Eq. (9) is, i.e., if the orbit bump is closed beyond the quadrupoles entering the discrete summation. In this case, simplified formulae useful for determining the major effects of $d_y(s), d'_y(s)$ and in particular their local extrema, can be derived ; they depend only on unperturbed first order optical parameters, which is convenient for estimating the effects of c.o. angle and off-centering from bare LHC optics.

We proceed by assuming a phase difference of $\pi/2\nu$ between the IP and neighboring low-β triplet quadrupoles i.e., $\sin[\nu(\phi(s_q) - \phi^*)] = \pm 1$, $\forall s_q$. The way things are worked out can be summarized as follows (see App. C for more details) : Eq. (10) is split in two distinct equations, that provide the solutions d_y^L and d_y^R from respectively the contributions of non-zero c.o. in the left- and right-hand side low-β triplets. The general solution is obtained by addition, $d_y(s) = d_y^L(s) + d_y^R(s)$ which after some algebra yields the following perturbative dispersion beyond the low-β triplets associated with the non-zero c.o. bump (s $< s_{q_L}$ $\forall q_L$, and $s > s_{q_R}$ $\forall q_R$),

$$\begin{aligned} d_y(s < s_{q_L}, s > s_{q_R}) &= -y_{co}(s) \\ &\pm y'^* \sqrt{\beta(s)\beta^*}/(2\sin\pi\nu) \sin\nu[\pi - |\phi(s) - \phi^*|] \sum (KL)_q \beta(s_q) \\ &\quad [\pm 1 \; for \; resp. \; \phi(s) \gtrless \phi(s_q), \forall q] \end{aligned} \tag{23}$$

Similar expression $d_y(s > s_{q_L}, s < s_{q_R})$ can be derived for the perturbation within the limits of the low-β triplet associated with the crossing (App. C, Eq. 54).

3.1 Crossing at a single IP

Simple expressions and relevant numerical results are drawn from Eq. (23). These can be verified to be in excellent agreement with MAD simulations, by means of the material provided in Appendix D. Note that $10^{-4} rad$ c.o. angle is taken ; it may be a conservative value in view of larger values mentioned in various publications. This is to be kept in mind when judging of the strength of correctors or harmfulness of the anomalous dispersion induced by crossing/off-centering schemes.

Extrema in the arcs

The extrema of the dispersion in the arcs can be obtained from Eq. (23) by taking $\sin\nu[\pi - |\phi(s) - \phi^*|] = 1$. On the other hand $y_{co}(s) = 0$ since the orbit bump is closed in the IR itself, while $\beta_{max}(s) \approx 180\, m/rad$ and $\sum (KL)_q \beta(s_q) \approx 370$ in odd-type IR's (App. B). This leads to $d_{x,extr}(arcs) < 0.228\, m$ for the horizontal plane ($\nu_x = 63.28$) that is, about 10% of the first regular order dispersion (which has 2.178 m peak value in the arcs) ; $d_{z,extr}(arcs) < 0.212\, m$ for the vertical plane ($\nu_z = 63.31$) (this is consistent with the results of section 2.2).

Extrema in low-β triplets

From Eq. (23) an expression for $d_y(s)$ in low-β triplets can be drawn. The phase there is $\phi(s) \approx \phi(IP) \pm \pi/2\nu$ practically independent of azimuth s at better than $10^{-2} rad$, which leads to

$$d_y[\phi(IP) \pm \pi/2\nu] \approx -y_{co}(s) \pm y'^* \sqrt{\beta(s)\beta^*}/(2\sin\pi\nu)\cos\nu[\pi - |\phi(IP) - \phi^*|] \sum (KL)_q \beta(s_q) \quad (24)$$

In particular, the extrema occur at β_{max} locations : in collision optics the numerical values of concern are $\beta^* = 0.5m$, $\beta(s) = 4430m$ at $IP1/5$, $4020m$ at $IP2/8$. Consider for instance horizontal c.o. angle $x'^* = 10^{-4} rad$ at $IP5$; the respective normalized betatron phases are (App. D) $\phi(IP1) = 0, \phi(IP2) = 2\pi 8.985/\nu_x, \phi(IP5) = \phi^* = \pi, \phi(IP8) = 2\pi 55.745/\nu_x$, and $\nu \equiv \nu_x = 63.28$. This yields (Fig. 1)

$$\begin{aligned} d_{x,extr}[\phi(IP1) - \pi/2\nu] &= 1.13m \; ; \quad d_{x,extr}[\phi(IP2) - \pi/2\nu] = 1.07m \; ; \\ d_{x,extr}[\phi(IP5) - \pi/2\nu] &= -0.71m \; ; \quad d_{x,extr}[\phi(IP8) - \pi/2\nu] = -1.05m \end{aligned} \quad (25)$$

Dispersion at IP's

Non-zero dispersion at IP results in beam size increase (see section 4.2). Eq. (23) with $\phi(s) = \phi(IP)$ and the phase values above provide

$$\begin{aligned} d_x(IP1) = 0 \; ; \; d_x(IP2) &= 1.08\,10^{-3}m \; ; \; d_x(IP8) = -2.58\,10^{-3}m \\ \textit{while} \quad d_x(IP5) = 1.38\,10^{-3}m \quad (Eq.\ 54) & \end{aligned} \quad (26)$$

For $\delta p/p = 10^{-4}$ these values of the dispersion give negligible beam size increase $d_x(IP)\delta p/p$.

Derivatives at IP's

Derivatives $d'_y[s = s(IP)]$ are of interest since they determine the amount of perturbation in the neighboring straight sections and low-β triplets (see section 4.2). Differentiation of Eq. (23) together with $y_{co}(IP) = 0, \alpha(IP) = 0, \beta(IP) = \beta^*$ leads to

$$d'_y[s(IP) \neq s^*] = y'^*/(2\sin\pi\nu)\cos\nu[\pi - |\phi(IP) - \phi^*|] \sum (KL)_q \beta(s_q) \quad (27)$$

For instance $x'^* = 10^{-4} rad$ c.o. angle at $IP5$ results in

$$d'_x(IP1) \approx -24.0\,10^{-3} rad, \; d'_x(IP2) \approx -23.9\,10^{-3} rad, \; d'_x(IP8) \approx -23.4\,10^{-3} rad \quad (28)$$

3.2 Interferences

The superposition principle results in interference when crossings are set at various IP's, between perturbative dispersion functions awaken at those IP's. These interferences may be either destructive or constructive, depending on the local phase, on the phase difference between IP's of concern and on the signs of the crossings.

Two-IP interference

Two-IP interference would occur for instance in the case of a pair of inclined crossing geometries, or four alternating crossings [11]. This can be illustrated as follows. Let $d_y^{IPa}(s > s_{q_R})$ be the dispersion induced downstream IPa by its crossing and $d_y^{IPb}(s < s_{q_L})$ that induced upstream IPb by its own.

The resulting dispersion all way from the right-hand side IPa low-β triplet through the left-hand side IPb low-β triplet writes (Eq. 23)

$$\begin{aligned} d_y^{IPa}(s > s_{q_R}) \quad + \quad & d_y^{IPb}(s < s_{q_L}) = -y_{co}^{IPa}(s) - y_{co}^{IPb}(s) - \sqrt{\beta(s)/(2\sin\pi\, nu)} \\ & \{y'(IPa) sqrt\beta(IPa)\sin\nu[\pi - \phi(s) + \phi(IPa)]\sum_{IPa}(KL)_q\beta(s_q) \\ - \quad & y'(IPb) sqrt\beta(IPb)\sin\nu[\pi + \phi(s) - \phi(IPb)]\sum_{IPb}(KL)_q\beta(s_q)\} \end{aligned} \tag{29}$$

Assuming identical optical design at both IP's we note, $\beta(IPa) = \beta(IPb) = \beta^*, \sum_{IPa}(KL)_q\beta(s_q) = \sum_{IPb}(KL)_q\beta(s_q) = \sum(KL)_q\beta(s_q)$, and $y'(IPa) = \epsilon y'(IPb) = y'^*$ ($\epsilon = \pm 1$). Eq. (30) simplifies to

$$\begin{aligned} d_y^{IPa}(s > s_{q_R}) \quad + \quad & d_y^{IPb}(s < s_{q_L}) = -[1+\epsilon]y_{co}(s) + y'^*\sqrt{\beta(s)\beta^*}/(2\sin\pi\nu) \\ \{ \quad & \sin\nu[\pi - \phi(s) + \phi(IPa)] - \epsilon\sin\nu[\pi + \phi(s) - \phi(IPb)]\,\}\sum(KL)_q\beta(s_q)\ (\epsilon = \pm 1) \end{aligned} \tag{30}$$

The extreme value in IPb (left-hand side) low-β triplet is obtained with $\phi(s) = \phi(IPb) - \pi/2\nu, \beta(s) = \beta_{max}$ i.e., neglecting $y_{co}(s)$

$$\begin{aligned} d_y, extr \quad = \quad & -y'^*\sqrt{\beta_{max}\beta^*} \\ & /(2\sin\pi\nu)\{\cos\nu[\pi - \phi(IPb) + \phi(IPa)] + \epsilon\cos\pi\nu\}\sum(KL)_q\beta(s_q)\ (\epsilon = \pm 1) \end{aligned} \tag{31}$$

Consider for instance interference between $IPa \equiv IP1$ and $IPb \equiv IP5$ for $z'^* = 10^{-4} rad$ vertical c.o. angle (such eventuality of vertical crossing has already been addressed [2] ; the interest is that vertical crossing allows arbitrary c.o. angle sign, which is suitable for our demonstration). The parameters of concern are $\phi(IP1) = 0$, $\phi(IP5) = \pi$, $\beta_{max} = 4430\,m$, $\beta^* = 0.5\,m$, $\nu \equiv \nu_z = 63.31$. The resulting extremum in $IP5$ low-β triplets is (Fig. 2)

$$\begin{aligned} d_{z,extr} = -z'^*\sqrt{\beta_{max}\beta^*}/(2\sin\pi\nu)(1+\epsilon\cos\pi\nu)\sum(KL)_q\beta(s_q) \quad (\epsilon = \pm 1) \\ yielding, \quad -z'^*\sqrt{\beta_{max}\beta^*}/(2\tan\pi\nu/2)\sum(KL)_q\beta(s_q) \approx 0.46\,m\ if \epsilon = +1 \\ and \qquad -z'^*\sqrt{\beta_{max}\beta^*}/2\tan\pi\nu/2\sum(KL)_q\beta(s_q) \approx 1.64\,m\ if \epsilon = -1 \end{aligned} \tag{32}$$

Note that, due to the fact that the two perturbations are not excited in phase there cannot be full cancellation (neither full addition) of amplitudes. These results clearly show the expectable mutual enhancement of harmful effects under multiple crossing or separation schemes in the absence of local correction.

Four-IP interference

Four non-alternating crossing configuration (i.e., all in the same plane) is also addressed in Ref.[11], though unlikely in view of long range tune shift effects. In such case strong effects may arise with adequate sign combinations. Consider horizontal c.o. angles $x'^* = \epsilon_{IP}\,10^{-4}$ with signs either identical, $\epsilon_1 = \epsilon_2 = \epsilon_5 = \epsilon_8 = 1$ or alternate, $\epsilon_1 = \epsilon_2 = 1$ and $\epsilon_5 = \epsilon_8 = -1$. Such combination is speculative since natural signs are rather $\epsilon_1 = \epsilon_5 = 1$ and $\epsilon_2 = \epsilon_8 = -1$; it entails secondary crossing between D1 and D2 and hence imposes vertical separation in order to avoid beam-beam interaction (this type of c.o. geometry is addressed in the hypothesis of so-called non-exchange crossing scheme, in

Ref.[2]). Assuming all sums $\sum(KL)_q\beta(s_q)$ take the same value at odd- and even-type IR's (in fact, respectively 370 and 350 - see App. B), calculations similar to the above [phases as for Eq. (26)] lead to extreme perturbation at $IP5$ left low-β triplet (Fig. 1 and App. D)

$$\begin{aligned} d_{x,extr} &= -x'^{*}\sqrt{\beta_{max}\beta^{*}}/(2\sin\pi\nu) \\ &\quad \sum_{IP=1-8}\epsilon_{IP}\cos\nu[\pi-|\phi(IP)-\phi(IP5)|]\sum(KL)_q\beta(s_q) \\ &\quad yielding,\ d_{x,extr}\approx 0.42\,m\ if\ all\ c.o.\ angles\ have\ identical\ signs \\ &\quad and,\ d_{x,extr}\approx 4.1\,m\ if\ \epsilon_1=\epsilon_2=1\ and\ \epsilon_5=\epsilon_8=-1 \end{aligned} \tag{33}$$

On the contrary the situation may improve at least locally for other combinations, as is the case with the natural signs $\epsilon_1=\epsilon_5=1$ and $\epsilon_2=\epsilon_8=-1$ which yield the extremum extremorum $d_{x,extr}=0.4\,m$ at $IP5$ low-β triplet. Fig. 3 shows the behavior of the perturbative dispersion in these three different cases. It is obtained from a 4-fold superposition of Eq. (23) with the simplifying hypothesis that all IP's are identical (same $\sum(KL)_q\beta(s_q)$, while homologous low-β quadrupoles have identical phase-shift w.r.t. the IP). The exact perturbed dispersion obtained with MAD is given in App. D.

4 Survey of the perturbative effects around the ring

4.1 Perturbative closed dispersion around LHC

Hereafter are displayed simulations and plots obtained by numerical calculations after section 2, using the unperturbed first order optical parameters of the LHC 4.2 optics (App. D). The intermediate values of the optical functions such as involved in the elementary kick summations or in the transport of the dispersion, are calculated from a MAD-TWISS output file, by means of dedicated software derived from the computer code RDTWISS [12].

In Fig. 1 are shown the perturbed closed dispersions D_x+d_x (horizontal) and d_z (vertical) as observed at various regions along the LHC ring, under the effect of respectively $x'^{*}=10^{-4}rad$ and $z'^{*}=10^{-3}m$ closed orbit geometry at $IP5$. The horizontal and vertical bumps are closed within Q4A.Left/Q4A.Right range, hence arising anomalous dispersion exclusively in the left- and right-hand side IR5 low-β triplets, as assumed in section 3.1. Detailed insight shows perfect agreement with MAD simulations (App. D). It can be observed that up to 1.13 m horizontal peak values are attained where the dispersion would be zero in the absence of c.o. bump. The second order horizontal dispersion $D_x(s)+d_x(s)$ shows an amplitude modulation in the arcs of $\pm10\%$ corresponding to the peak perturbation $d_{x,extr}(s)(\pm0.2\,m$ introduced by the crossing optics.

The next two figures show interferencial effects. The building up of perturbative closed dispersion under the effect of a two-IP interference, as observed along Octant 5, is displayed in Fig. 2. Vertical c.o. angles $z'^{*}(IP1)=10^{-4}rad$ and either $z'^{*}(IP5)=10^{-4}rad$ or $z'^{*}(IP5)=-10^{-4}rad$ are taken. The interference is obtained by superposition ${}^{1}d_z(s)+{}^{5}d_z(s)$ and ${}^{1}d_z(s)-{}^{5}d_z(s)$ of the independent solutions ${}^{1}d_z(s)$ and ${}^{5}d_z(s)$ of Eq. (8) obtained under single crossing at respectively $IP1$ and $IP5$. Figure 3. shows the effects of four-IP interference as observed at Octant 5. All crossings are in the horizontal plane with an angle $x'^{*}=\epsilon_{IP}\,10^{-4}rad$, and various sign combinations, namely $\epsilon_1=\epsilon_2=\epsilon_5=\epsilon_8=1$, $\epsilon_1=\epsilon_2=1$ and $\epsilon_5=\epsilon_8=-1, \epsilon_1=\epsilon_5=1$ and $\epsilon_2=\epsilon_8=-1$. The interference is obtained by four-fold superposition of the solutions of Eq. (8).

4.2 Beam size related effects

Beam-beam separation

The normalized beam-beam separation expresses as

$$d_{sep}(s) = \frac{distance\,between\,beam\,centroids}{max[\sigma(s)]} = \frac{2y'^{*}s}{max[\sigma(s)]},$$

where $max[\sigma(s)]$ is the size of the largest beam at distance s from the IP and $2y'^{*}$ is the c.o. angle (y stands for either x or z ; results stated below are valid for both planes as long as the first order horizontal dispersion is zero in the IP straight section). Increased beam size $\sigma(s)$ in the IP region therefore entails smaller normalized separation and results in tune shift and tune spread which both scale as $d_{sep}^{-2}(s)$. The effect of non-zero dispersion is of concern in this respect since the $\sigma^2(s)$ writes

$$\sigma^2(s) = \beta(s)\epsilon/\pi + [d_y(s)\delta p/p]^2 \tag{34}$$

where ϵ/π is the r.m.s. emittance, $\delta p/p$ is the r.m.s. momentum spread and $d_y(s) = s\,d'_y(IP)$ can be obtained from Eq. (27). However the anomalous dispersion is weak enough that its effect can be neglected. Indeed, in the long range approximation ($s >> \beta^*$) in the IP straight section one has $\beta(s) \approx s^2/\beta^*$ which leads to $\sigma^2(s) = s^2\{1/\beta^* + [d'_y(s)\delta p/p]^2\}$ and hence

$$d_{sep}^2(s) \approx 4y'^{*2}/\{\epsilon/\pi/\beta^* + [d'_y(s)\delta p/p]^2\} \tag{35}$$

In collision optics the figures of concern are on the one hand $\beta^* = 0.5\,m/rad$ and $\epsilon/\pi \approx 5\,10^{-10} m.rad$ giving $\epsilon/\pi/\beta^* \approx 10^{-9}$, on the other hand $d'_y(s) < 0.03\,rad$ under single $\pm 10^{-4} rad$ c.o. angle and $\delta p/p = 10^{-4}$ giving $[d'_y(s)\delta p/p]2 < 10^{-11}$. It results that $d_{sep}^2(s) \approx 4y'^{*2}\beta^*/\epsilon/\pi$ independent of the anomalous dispersion at better than 1%.

Luminosity

The luminosity scales as $1/\sigma_x^*\sigma_z^*$ while the effect of momentum dispersion on $\sigma_{x,z}^*$ is given by Eq. (34). In the absence of compensation the dispersion at IP does not exceed $3\,10^{-3}m$ (Eq. 26) with negligible effect of the derivative (Eq. 28) over the $7.5\,10^{-2}m$ bunch length at 7 TeV. In consequence $\beta^*\epsilon/\pi \approx (16\,10^{-6}m)^2 >> [d_{x,z}(IP)\delta p/p]^2 \approx (0.3\,10^{-6}m)^2$ and practically $\sigma_{x,z}^* \approx \beta_{x,z}^*\epsilon/\pi$ independently of any correction of the anomalous dispersion.

Mechanical aperture

The mechanical aperture related to betatron motion and momentum dispersion writes (Ref.[1], p.38) $A = (\sigma + D_x\delta p/p)k + \delta_{sep}$ where $\sigma = \sqrt{\beta\epsilon/\pi}$, δ_{sep} = beam-beam separation in common vacuum pipes, and $k \approx 1.1$ accounts for optics errors. As shown above the anomalous dispersion already eats up 10% D_x which means that the contribution of dispersion to k is doubled if no compensation is introduced. In the low-β triplets the additional term δ_{sep} is obtained from the c.o. geometry and culminates at about $4.7\,10^{-3}m$ for 10^{-4} c.o. angle, the anomalous dispersion enhances it by up to $10^{-4}m$ for $\delta p/p = 10^{-4}$ (collision energy, single crossing) that is, about 2%.

Non linearities

Anomalous dispersion introduced by $10^{-4} rad$ c.o. angle increases the n-σ transverse excursion of off-momentum particles by up to about $n\,10^{-4}(m)$ at the location of maximum c.o. (inside Q2 or QT.Q3). Considering that multipole feed-down due to the non-zero c.o., unless compensated, is presumed to have sensible effect on the dynamic aperture [13], the effect of d_x in this respect deserves finer insight.

5 Correction schemes

The effects of the perturbative closed dispersion are significant enough that their compensation be worth investigating. Yet their limited amount suggests that natural absorption of the horizontal component of the anomalous dispersion within regular IR tuning procedures is achievable ; main aspects of this are given in section 5.1. Section 5.2 shows the feasibility and efficiency of a correction method proposed for SSC [14] ; it is made attractive by its compatibility with the so-called modular tuning of the IR [10] and other Q-shift procedures [15] ; some remarks follow concerning single- or double-quadrupole compensation. Section 5.3 discusses gain expectable from interference, as pointed out in section 3.2. Section 5.4 presents the application of skew quadrupole correction scheme [14] to vertical crossing.

5.1 Self-absorption within regular IR tuning procedures

In presence of horizontal crossing/off-centering at an IP the total dispersion is the sum $D_x(s)+d_x(s)$ of the regular first order dispersion introduced by the main dipoles and the anomalous dispersion waken by non-zero c.o. in the low-β quadrupoles. $D_x(s) + d_x(s)$ is nothing else than the second order dispersion and can be handled and matched straightforwardly with MAD [4] since the code performs second order transport. Typical IR tuning procedures as used here, relevant in particular with the Version 4 of LHC ring, can be found in Ref.[16] ; they result in what follows.

The left column in Table 1 shows the odd-IR quadrupole strengths in collision optics for the bare LHC Version 4.2 optics [5] ; the right column shows their values in presence of $x'^* = 10^{-4} rad$ c.o. angle, after re-tuning the IR to the usual matching constraints (recovering the arcs periodic functions at IR ends, and optical functions at IP), which are attained in the present case with a penalty $< 10^{-21}$, signature of adequate fulfillment (the match file is that used in Ref.[16], it is given in App. E). As expected from $d_x(s) \approx 10\% D_x(s)$ under $\pm 10^{-4} rad$ c.o. angle (see section 3), the Q1-Q10 quadrupole strength variations from non-crossing to crossing is very limited. Figure 4 displays the betatron and second order dispersion functions across the IR in presence of the c.o. angle, after re-tuning of the IR ; the main difference w.r.t. regular optics is in the non-zero dispersion in the low-β triplets . Table 2 shows such ensuing parameters as the optical functions at $IP1, 2, 5, 8$, tunes and other β_{max} obtained from a one-turn MAD TWISS procedure : there is no meaningful difference with the unperturbed ones ; it is clear that any remaining mismatch is negligible, otherwise one or the other of these parameters would be sensibly affected.

Table 1: Odd-IR quadrupole strengths that fulfill the regular constraints in collision optics [16], without (left column) and with (right column) crossing ($10^{-4} rad$ horizontal c.o. angle at $IP5$).

Quadrupole name name	Original strength (m^{-2})	Strength after re-tuning (m^{-2})
KQT10.L5	-1.046017E-03	-9.771783E-04
KQT9.L5	2.787685E-03	3.143025E-03
KQT8.L5	-3.342663E-03	-4.217364E-03
KQT7.L5	2.578090E-03	3.139576E-03
KQ6L5	-7.224747E-03	-7.129641E-03
KQ5.L5	8.043164E-03	8.037628E-03
KQ4.L5	-9.778419E-03	-9.971877E-03
KQT3.L5	4.267829E-03	4.301427E-03
KQT1.L5	3.424101E-03	3.437690E-03
KQ1.L5	9.725345E-03	9.717873E-03

Table 2: Optical functions at $IP1, 2, 5, 8$ and other parameters obtained from a one-turn MAD

pos.	lmnt	betax betay [m]	alfax alfay [1]	mux muy [2pi]	x(co) y(co) [mm]	px(co) py(co) [.001]	Dx Dy [m]	Dpx Dpy [1]
1	$IP1$	0.500	0.000	0.000	0.000	0.000	0.000	0.000
		0.500	0.002	0.000	0.000	0.000	0.000	0.000
599	$IP2$	0.500	0.000	8.985	0.000	0.000	0.000	0.000
		0.500	-0.003	7.540	0.000	0.000	0.000	0.000
2409	$IP5$	0.500	0.000	31.657	0.000	0.100	0.000	0.000
		0.502	-0.002	31.639	0.000	0.000	0.000	0.000
4198	$IP8$	0.500	0.000	55.745	0.000	0.000	0.000	0.000
		0.500	0.004	54.322	0.000	0.000	0.000	0.000
Qx = 63.280035					Qy = 63.310027			
betax(max) = 4431.634796					betay(max) = 4430.698831			
Dx(max) = 2.177799					Dx(r.m.s.) = 1.501178			
xco(max) = 4.706675								

5.2 Quadrupole correction of the horizontal dispersion

Corrector strength

In the formalism of section 2 the quadrupole correction method consists in waking a perturbative dispersion which interferes destructively with that due to a low-β triplet. It can be applied independently to the left and right triplets, with distinct corrector strengths having distinct strengths since both triplets induce unequal kicks. Note that there is no obligation to do so, namely the overall dispersion resulting from additive effect of the two triplets can be canceled with a single quadrupole having the full compensating strength.

Adding quadrupole corrector(s) to the structure results in the additional term $\int K_Q(s)d_x(s)\delta(s-s_Q)ds_Q$ in Eq. (7) (the index Q stands for the correctors). The solution (Eq. 8) is to be added the complementary term

$$\sqrt{\beta_x(s)}/(2\sin\pi\nu)\sum_Q(KL)_Q D_x(s_Q)\beta_x(s_Q)\cos\nu[\pi-|\phi(s)-\phi(s_Q)|]$$

whose role is to balance the closed orbit effect. This leads to the compensation condition

$$\sum_Q(KL)_Q D_x(s_Q)\sqrt{\beta_x(s_Q)}\cos\nu[\pi-|\phi(s)-\phi(s_q)|]$$
$$-\sum_q(KL)_q x_{co}(s_q)\sqrt{\beta_x(s_q)}\cos\nu[\pi-|\phi(s)-\phi(s_q)|]=0 \tag{36}$$

beyond the corrector/triplets range. Besides, in order to minimize the corrector strength, on the one hand the phase shifts should verify $\phi(s_Q)=\phi(s_q)+\pi/\nu[\pi/\nu]$ [1] ; on the other hand $D_x(s_Q)\sqrt{\beta_x(s_Q)}$ should be maximized, which also minimizes effects on the orthogonal plane ; considering $\phi(s_q)$ and $D_x(s_Q)\sqrt{\beta_x(s_Q)}\approx C^{ste}$ this leads to

$$|\sum_Q(KL)_Q|=|\sum_q(KL)_q x_{co}(s_q)\sqrt{\beta_x(s_q)}\ /\ D_x(s_Q)\sqrt{\beta_x(s_Q)}| \tag{37}$$

with sign depending on the phase shift from corrector to triplet (cosine term in Eq. (36)). Note that, within the corrector/triplet range the effect of the absolute values in Eq. (36) results in

[1] Modulo π/ν

the compensation condition being not fulfilled which entails residual dispersion modulation. Numerical calculations give (App. B), in odd IR for respectively the left and right low-β triplets $\sum(KL)_q x_{co}(s_q)\sqrt{\beta_x(s_q)}|_{Left/Right} = -1.12\,10^{-2}/1.50\,10^{-2}$, while the correctors are at locations where (Table 3) $D_x(s_q)\beta_x(s_q)|_{Left/Right} \approx 29$. Hence the typical integrated strengths necessary to independently close the left and right dispersion bumps are (Eq. 37)

$$|(KL)_Q|_{Left/Right}| \approx 3.9\,10^{-4}/5.2\,10^{-4} m^{-1} \tag{38}$$

Correction with a single quadrupole

A single quadrupole is sufficient in principle to cure the anomalous dispersion, for the reason that the two low-β triplets sources of the defect are with good precision π/ν from each other, therefore exciting independently perturbations that add in phase beyond the IP straight section. It may be placed close to a MSCBH multipole (in the notations of lhc42.sequence MAD file [5]) at $D_x(s_q)\beta_x(s_q)|_{Left/Right} \approx 29$ (Table 3) about $\pi/\nu[\pi/\nu]$ away from the triplets and would excite a defect with equal amplitude and opposite sign which would cancel the anomalous dispersion beyond the local chromatic bump so determined (Fig. 5). Its strength needs be $|(KL)_Q| \approx 3.9\,10^{-4} + 5.2\,10^{-4} \approx 9\,10^{-4} m^{-1}$ (Eq. 38). A single quadrupole though would have sensible effect on the tune and β mismatch, namely (Fig. 5)

$$\begin{aligned} \Delta\nu &= \beta(s_Q)(KL)_Q/4\pi \\ &\approx 1.3\,10^{-2} \textit{ in the plane of the dispersion correction, taking } \beta(s_Q) = 178\,m, \\ &\approx 0.23\,10^{-2} \textit{ in the other plane, taking } \beta_(s_Q) = 32\,m \end{aligned} \tag{39}$$

$$\begin{aligned} \Delta\beta(s)/\beta &= \beta(s_Q)|(KL)_Q \cos 2\nu[\pi - |\phi(s) - \phi(s_Q)|]|/2\sin(2\pi\nu) < \beta(s_Q)|(KL)_Q|/2\sin(2\pi\nu) \\ &\approx \pm 8.5\% \textit{ in the plane of the dispersion correction, taking } \nu \approx 63.3, \\ &\approx \pm 1.5\% \textit{ in the other plane, taking } \nu \approx 63.3 \end{aligned} \tag{40}$$

Correction with two quadrupoles

These undesirable effects can be taken care of beyond the IR by using two quadrupoles instead of just one, placed at locations of equal $\beta(s_Q)$, distant $\pi/\nu[2\pi/\nu]$ from one another, both $\pi/\nu[\pi/\nu]$ away from the low-β triplets. This could constitute a minimal correction scheme. In such case there are three possibilities.

The two quadrupoles can be placed one at each end of the IR, with each one half the strength $|(KL)_Q/2| \approx 4.5\,10^{-4} m^{-1}$. This has the effect of avoiding tune-shift since in this case $\beta(s_Q)(KL)_Q/4\pi = 0$ (Eq. 39) and β-beats since $\beta(s_Q)|(KL)_Q \cos 2\nu[\pi - |\phi(s) - \phi(s_Q)|]| \approx 0$ (Eq. 40). On the other hand, this precludes balancing on each side of the IP between the correctors and the corresponding low-β triplets which are defect sources of unequal strengths ($\sum(KL)_q x_{co}(s_q)\beta_x(s_q)|_{Left} \neq \sum(KL)_q x_{co}(s_q)\beta_x(s_q)|_{Right}$, Eq. 38) ; this results in a dispersion bump localized between the two correctors and in particular unmatched dispersion values at IP (Fig. 6) ; however this residual effect is weak and zero dispersion and derivative at the IP can be recovered by slight re-tuning of the IR. It also leaves residual effects beyond the IR, such as betatron beating in the arcs (up to 2.8%, due to the two quads being not exactly $\pi/\nu[2\pi/\nu]$ distant), dispersion beating in the arcs [less than $\pm 1\%$, to be compared to $\pm 10\%$ in the absence of correction, see Fig. (1)].

The two quadrupoles can be placed one at each end of the IR, with strengths balancing the corresponding low-β triplet, namely (Eq. 38)

$$(KL)_{Q.Left\ /\ Right} = \sum (KL)_q x_{co}(s_q)\beta_x(s_q)|_{Left\ /\ Right} \approx 3.9\,10^{-4}\ /\ 5.2\,10^{-4} m^{-1} \qquad (41)$$

This has the effect of leaving some tune-shift $\Delta\nu = \sum_Q \beta(s_Q)(KL)_Q/4\pi \approx 1.8\,10^{-3}$ in the horizontal plane, $3.2\,10^{-4}$ in the vertical plane (Eq. 39) and β-beats $\sum_Q \beta(s_Q)|(KL)_Q \cos 2\nu[\pi - |\phi(s) - \phi(s_Q)|]| \lesssim 1.2\%$ in the plane of the correction (Eq. 40). On the other hand, this balances exactly each low-β triplet on each side of the IP and results in quasi-zero dispersion and derivative at the IP (Fig. 7).

The two quadrupoles can be placed at the same end of the IR, with each one half the strength $|(KL)_Q/2| = 4.5\,10^{-4} m^{-1}$. This has the effect of avoiding tune-shift and β-beats, while $D_x \approx 9\,10^{-3}\,m$ and $D_x^{'} < 510^4 rad$ (Fig. 8).

Interlaced correction scheme

Following a correction scheme proposed for SSC [14], we extend the considerations above to two double pair of quadrupoles placed at the IR ends. Such correction scheme is also assimilable within the recently developed LHC IR tuning scheme [10] and other Q-shift system [15]. Indeed, these last are to handle in particular the dispersion due to the separator/recombiner dipoles D1/D2, while the crossing optics amount to about 35% their effect (under single $\pm 10^{-4} rad$ c.o. angle, see section 2.3).

The scheme and the role of the additional two quadrupole pairs w.r.t. what precedes can be summarized as follows. A quadrupole corrector is placed π/ν (normalized phase-shift) away from the low-β triplet source of the perturbation, at a location of high $D_x\sqrt{\beta_x}$ so as to maximize its efficiency and low β_z in order to insure decoupling. Its effect is to close the second order dispersion bump opened in the low-β triplet. In fact, the phase-shift between the corrector and the low-β triplet cannot presumably be exactly π/ν, there must therefore be a companion corrector, about $\pi/2\nu$ distant. Moreover, such quadrupole compensation would have sensible effect on the betatron functions ; this is avoided by using, instead of single quadrupoles, pairs of quadrupoles π/ν apart, of opposite sign and half the necessary strength. Not much more needs be said about the method, which is abundantly documented in Refs.[10,13].

We investigate an interlaced geometry, in complement to what was done previously about the D1/D2 separators [10]. In the present simulations the quadrupole correctors are "INSTALL'ed" (MAD option [4]) next to the multipoles MSCBH in the LHC sequence (lhc42.sequence MAD file [5]), at $D_x(s_Q)\beta_x(s_Q) \approx 29$ (Table 3, column 3) close to its maximum value. The integrated correcting strength is matched with MAD with constraints exclusively on $D_x = 0$ and $D_x' = 0$ at IP and Octant ends. The strength is essentially in the HQ1a/b.Left and HQ1a/b.Right pairs (Eq. 38 and column 5 of Table 3) ; their positioning coincides with almost $\pi/2\nu[\pi/\nu]$ distance from the IP, on respectively the left- and right-hand side of the IR (by QF13/17.Left and QF12/16.Right). The weak role of HQ2a/b.Left and HQ2a/b.Right companion pairs (distant almost $\pi/\nu[\pi/\nu]$ from the IP, on respectively the left- and right-hand side of the IR, by QF15/19.Left and QF10/14.Right) is shown in Table 3 (column 5) ; they however do help canceling residual perturbative dispersion (up to 0.12 m and 0.30 m peaks remain in IR1 and IR5 low-β triplets if they are off) and should be used in order to get clean compensation.

With the four pairs the correction of the dispersion is very efficient. The main difference w.r.t. the original machine parameters (see Table 4) is in the peak value of the second order dispersion, namely $D_x(max) = 2.373$ m instead of 2.178 m ; it is due to the modulation within the chromatic bump and takes place by QF11.Left and Q10.Right. The residual dispersion beating in the arcs is negligible (Fig. 9). The absence of effect on the first order focusing is apparent in Table 4 which displays the ensuing values of the optical functions at $IP1, 2, 5, 8$, as well as tunes and other parameters as obtained from a one-turn MAD TWISS procedure without any additional re-tuning of the IR ; it is clear that any induced mismatch is negligible, otherwise some of these parameters would be sensibly

Table 3: Corrector strengths necessary for canceling the chromatic bump opened in the left and right odd-type low-β triplets by the non-zero horizontal c.o. due to $x'^* = 10^{-4} rad$ c.o. angle at IP, as obtained from a MAD match. The correctors are all placed next to the lattice multipole correctors at high $D_x(s_Q)\beta_x(s_Q)$ values (column 3). The pairs HQ1a/b.Left and HQ1a/b.Right are almost $\pi/\nu[\pi/\nu]$ distant from respectively the left- and right-hand side low-β triplets (column 4), they play the dominant role, with integrated strengths $(KL)_q|_{Left/Right} = -3.86\,10^{-4}/-5.08\,10^{-4} m^{-1}$ [twice the value in column 5, consistent with Eq. (38)] ; the pairs HQ2a/b.Left and HQ2a/b.Right are almost $\pi/2\nu[\pi/\nu]$ distant from respectively the left- and right-hand side low-β triplets, and have weak role as expected (column 5).

Corrector name	Neighboring quadrupole	$D_x(s_Q)\sqrt{\beta_x(s_Q)}$ $(m^{3/2})$	Phase w.r.t. IP $(\pi/2\nu)$	$(KL)_Q$ $(10^{-4}m^{-1})$
HQ2a/b.Left	QF15/19.Left	29	-1.517 / -2.018	$\pm$ 0.22
HQ1a/b.Left	QF13/17.Left	29	-1.266 / -1.767	$\pm$ 1.93
HQ1a/b.Right	QF10/14.Right	29	1.782 / 2.284	$\pm$ 2.54
HQ2a/b.Right	QF12/16.Right	29	1.531 / 2.033	$\mp$ 0.56

Table 4: Optical functions at $IP1, 2, 5, 8$ and other parameters obtained from a one-turn MAD TWISS procedure in presence of the quadrupole corrector pairs tuned as shown in Table 3, without any additional re-tuning of the IR.

pos.	lmnt	betax betay [m]	alfax alfay [1]	mux muy [2pi]	x(co) y(co) [mm]	px(co) py(co) [.001]	Dx Dy [m]	Dpx Dpy [1]
1	*IP*1	0.500	0.000	0.000	0.000	0.000	0.000	0.000
		0.500	0.001	0.000	0.000	0.000	0.000	0.000
599	*IP*2	0.500	0.000	8.985	0.000	0.000	0.000	0.000
		0.501	-0.003	7.540	0.000	0.000	0.000	0. 000
409	*IP*5	0.501	0.000	31.640	0.000	0.100	0.000	0.000
		0.502	-0.001	31.655	0.000	0.000	0.000	0.000
198	*IP*8	0.500	0.000	55.745	0.000	0.000	0.000	0.000
		0.500	0.003	54.322	0.000	0.000	0.000	0.000
Qx = 63.280014					Qy = 63.31000			
betax(max)= 4433.444055					betay(max) = 4430.143142			
Dx(max) = 2.373266					Dx(r.m.s.) = 1.504751			
xco(max) = 4.707107								

affected. The horizontal and vertical β-beating in the arcs are respectively $\pm 0.15\% and \pm 0.5\%$ (Fig. 9), and the machine tunes are not affected.

5.3 Partial compensation from interference

Interference with D1/D2

One aspect of interference is the expectable gain in corrector strength for the case of compensation of D1/D2 by quadrupole pairs placed at the IR ends [10]. With the right sign of crossing at the corresponding IP, the necessary strength can be decreased by about 35% (Eq. 21), as schemed in Fig. (10). The reason for this simple behavior is that D1/D2.Left (respectively D1/D2.Right) is at the same betatron phase than the left (respectively right) low-β triplet source of the anomalous dispersion.

Interference between IP1 and IP5, or IP2 and IP8

Also, as pointed out in section 3.2 some amount of mutual compensation is to be expected upon in-

terference of perturbative closed dispersions excited by crossing or off-centering geometry at distinct IP's. However since IP's are not distant $\pi/\nu[\pi/\nu]$ the two perturbations cannot exactly cancel each other (Fig. 2), yet the overall effect may locally be beneficial with the adequate c.o. signs. Main features can be summarized as follows.

In the vertical plane for instance, the peak perturbation under $10^{-4} rad$ c.o. angle at $IP1$ occurs in $IP5$ low-β triplet with about 1.05 m (after section 3.1 and Fig. 1). It comes out from section 3.2 that this peak goes down to $d_{x,extr}[\phi(IP1) - \pi/2\nu] + d_{x,extr}[\phi(IP5) - \pi/2\nu] = 1.05(1 + \cos\pi\nu) \approx 0.46\, m$ (Eq. 33) if crossings are set simultaneously with identical signs at $IP1$ and $IP5$. The extremum of the modulation in the arcs (which occurs in Octant 5), given in the single crossing case by $\bar{D}_z|_{z^*} = 0\sqrt{\beta(s)} \approx 158 z'^* \sqrt{\beta(s)} \approx 0.21\, m$ (Eq. 14) decreases slightly down to 0.19 m if there is interference (Fig. 11). Similar considerations hold for the even-type IR's 2 and 8. Again they are not $\pi/\nu[\pi/\nu]$ distant, yet the interferencial damping factor in the low-β triplets $\{\cos\nu[\pi - \phi(IPb) + \phi(IPa)] + \cos\pi\nu\} \approx (\cos\pi\nu/2 + \cos\pi\nu) \approx 0.09$ (Eq. 32) is five times more favorable than the above odd-type IR's one $(1 + \cos\pi\nu) \approx 0.44$ (Fig. 12). Identical behavior occurs in the horizontal plane, to be superposed onto the regular first order dispersion.

The interest of such interferencial compensation is that, although it does not provide full cancellation it however damps the anomalous dispersion to values low enough to consider living with. In any case it is totally transparent for the focusing and avoids the side effects that accompany corrector based methods.

5.4 Correction of the vertical dispersion with skew quadrupoles

Correction of the vertical dispersion can be attempted with either dipole correctors or skew quadrupole correctors. Both solutions have been already investigated, in the case of SSC. The former was to be abandoned, mostly in view of harmful effects entailed by the so induced extended non-zero closed orbit. Similar attempts have been performed as to LHC, not reported here, with the same drawbacks ; the more flexible Version 5 of the optics [17] might be worth more investigations in this way. However, following the correction scheme based on skew quadrupoles [14], the vertical anomalous dispersion can be compensated by arrangement of corrector pairs located at the neighboring arc ends. The philosophy is similar to what is done for the horizontal anomalous dispersion in section 5.2. These skew quadrupoles couple the horizontal dispersion to the vertical plane ; they must be placed at maxima of $D_x\sqrt{\beta_z}$ in order to minimize their strength, yet at as low as possible β_x in order to minimize perturbations in the horizontal plane. These constraints are to meet those on the phase, as for the horizontal plane, namely, at each end of the IR a quadrupole pair is to be placed about π/ν (normalized phase-shift) away from the low-β triplet source of the perturbation, with a companion pair about $\pi/2\nu$ distant in order to achieve perfect compensation of the vertical anomalous dispersion. Note that just as for the horizontal dispersion, due to the special phase properties of the LHC IR optics, the correction scheme can again be simplified to a single or two skew quadrupoles, as described below. The necessary strength in the correctors can be estimated as follows.

Corrector strength

Following the notations of section 2, adding skew quadrupole corrector(s) of strength R(s) to the structure results in coupled motion which is described as for its vertical component by (see section 2 for the notations)

$$d^2z/ds^2 + K(s)z - R(s)x = 0 \tag{42}$$

The ensuing equation to solve for $d_z = z/\delta$ writes

$$d^2d_z/ds^2 + K(s)d_z = R(s)D_x \tag{43}$$

Table 5: Optical functions at $IP1,2,5,8$ and other parameters obtained from a one-turn MAD TWISS procedure in presence of a single skew quadrupole corrector placed at QD12.L5, without any additional re-tuning of the IR.

pos.	lmnt	beta1 beta2	alfa1 alfa2	mu1 mu2 [2pi]	R11 R21	R12 R22	xco yco [mm]	pxco pyco [.001]	Dx Dy	Dpx Dpy
1	IP1	0.499	0.022	0.000	-0.171	-0.121	0.000	0.000	0.000	0.000
		0.512	0.010	0.000	0.552	-0.225	0.000	0.000	0.002	-0.001
599	IP2	0.501	0.022	8.985	0.069	0.149	0.000	0.000	0.000	0.000
		0.509	0.016	7.539	-0.646	0.128	0.000	0.000	-0.002	0.002
2411	IP5	0.511	-0.002	31.638	-0.245	-0.109	0.000	0.000	0.000	0.000
		0.502	-0.025	31.662	0.520	-0.197	0.000	0.100	0.006	-0.003
4200	IP8	0.504	0.021	55.741	0.090	0.142	0.000	0.000	0.000	0.000
		0.511	0.016	54.325	-0.652	0.137	0.000	0.000	0.002	-0.001
Q1 = 63.276573						Q2 = 63.313657				
betax(max)= 4443.434002						betay(max) = 4415.146173				
Dx(max) =2.180507						Dy(max) = 0.321702				
yco(max) = 4.707107										

(the vertical anomalous dispersion $d_z(s)$ is neglected, or as well considered already corrected). This differential equation is identical to Eq. (5) (obtained by changing d_z to d_y and $R(s)D_z$ to $K(s)y_{co}$) hence its solution is [after Eq. (8)]

$$d_z(s) = \sqrt{\beta_z(s)}/(2\sin\pi\nu_z)\sum(RL)_{SQ}D_x(s_{SQ})\sqrt{\beta_z(s_{SQ})}\cos\nu[\pi - |\phi(s) - \phi(s_{SQ})|] \tag{44}$$

where the discrete sum extends over index SQ which denotes the correctors, ϕ is the normalized vertical betatron phase. The compensation condition writes (see section 5.2)

$$\sum_q (KL)_q z_{co}(s_q)\sqrt{\beta_z(s_q)}\cos\nu_z[(-|\phi(s) - \phi(s_q)|]$$
$$-\sum_{SQ}(RL)_{SQ}D_x(s_{SQ})\sqrt{\beta_z(s_{SQ})}\cos\nu_z[\pi - |\phi(s) - \phi(s_{SQ})|] = 0 \tag{45}$$

where the index q designates the low-β triplet quadrupoles. Now, on the one hand the approximation $\phi(s_{SQ}) = \phi(s_q) + \pi/\nu[\pi/\nu]$ while $\phi(s_q) \approx C^{ste}$ still holds ; on the other hand as shown below $D_x(s_{SQ})\sqrt{\beta_z(s_{SQ})} \approx C^{ste}$, which leads to

$$|\sum_S Q(RL)_{SQ}| = |\sum_q (KL)_q z_{co}(s_q)\sqrt{\beta_z(s_q)} \ / \ D_x(s_{SQ})\sqrt{\beta_z(s_{SQ})}| \tag{46}$$

with sign depending on the phase shift $\pi/\nu[\pi/\nu]$ from corrector to triplet. Note that the compensation condition is not fulfilled within the corrector/triplet range which entails residual dispersion modulation. Numerical calculations (App. B) give, in odd-type IR for respectively the left- and right-hand side low-β triplets $\sum(KL)_q z_{co}(s_q)\sqrt{\beta_z(s_q)}|_{Left/Right} = -1.50\,10^{-2}/1.12\,10^{-2}$, while at correctors locations $D_x(s_{SQ})\sqrt{\beta_z(s_{SQ})}|_{Left/Right} \approx 14$ (Table 9, column 3). Hence the integrated strengths necessary to independently close the left and right dispersion bumps are (Eq. 46)

$$|(RL)_{SQ}|_{Left/Right}| \approx 10.6\,10^{-4}/7.9\,10^{-4}m^{-1} \tag{47}$$

Correction with a single skew quadrupole

Table 6: Optical functions at $IP1, 2, 5, 8$ and other parameters obtained from a one-turn MAD TWISS procedure in presence of two skew quadrupole corrector placed respectively at QD12.L5 and QD17.R5 with opposite strengths, prior to any re-tuning of the IR.

pos.	lmnt	beta1 beta2	alfa1 alfa2	mu1 mu2 [2pi]	R11 R21	R12 R22	xco yco [mm]	pxco pyco [.001]	Dx Dy	Dpx Dpy
1	IP1	0.500	-0.001	0.000	0.009	-0.004	0.000	0.000	0.000	0.000
		0.501	0.001	0.000	-0.013	-0.007	0.000	0.000	0.000	0.000
599	IP2	0.500	-0.001	8.985	-0.009	0.004	0.000	0.000	0.000	0.000
		0.501	-0.003	7.540	0.016	0.006	0.000	0.000	0.000	0.001
2411	IP5	0.500	0.000	31.640	-0.053	0.022	0.000	0.000	0.000	0.000
		0.502	-0.001	31.655	0.006	0.001	0.000	0.100	-0.002	-0.003
4202	IP8	0.500	-0.001	55.745	-0.011	0.003	0.000	0.000	0.000	0.000
		0.501	0.003	54.322	0.011	0.008	0.000	0.000	0.000	-0.001
Q1 = 63.280131						Q2 = 63.310120				
betax(max)= 4432.261623						betay(max) =4426.964313				
Dx(max) = 2.178097						Dy(max) = 0.180680				
yco(max) = 4.707107										

Things are similar to what has been discussed about the horizontal dispersion (Section 5.2). The skew quadrupole is placed by QD12.L5 at the arc end, with strength $(RL)_{SQ} = 18.2\,10^{-4}m^{-1}$ (after Eq. 47) ; MAD simulations with the sole constraint DY = DPY = 0 outside the bump provides identical strength. The tune shifts are respectively $\Delta\nu_x = -\Delta\nu_z \approx -3.4\,10^{-3}$ while $\Delta\beta_{x,z}/\beta_{x,z} < \pm 3\%$ (Table 5). The dispersion is damped from 0.71 m (Fig.1 and Eq. 26) to 0.32 m at the crossing IR, to less than 0.12 m in the other IR's (where it was of the order of 1 m), and less than 0.05 m in the arcs. Relevant graphs are shown in Fig. 13.

Correction with two skew quadrupoles

As for the horizontal dispersion there are several possibilities in positioning the quadrupoles, more or less beneficial in terms of residual dispersion, tune shift and β-beat. Things can be summarized as follows.

Fig. 14 and Table 6 show the optical functions when the quadrupoles are placed one at each arc end (QD12.L5 and QD17.R5 respectively) with opposite strengths $(RL)_{SQ}/2 = \pm 9.1\,10^{-4}m^{-1}$. In particular the residual dispersion is about 0.12 m in the crossing triplet, less than 0.12 m in the other IR's, and less than 0.05 m in the arcs.

Fig. 15 and Table 7 show the optical functions when the quadrupoles are placed one at each arc end (QD12.L5 and QD17.R5 respectively) with distinct strengths $(RL)_{SQ}|_{Left/Right}| \approx 10.6\,10^{-4}/-7.9\,10^{-4}m^{-1}$ balancing the respective strength of the opposite low-β triplet. The residual dispersion is 0.22 m in the crossing triplet and zero everywhere beyond the crossing IR.

Fig. 16 and Table 8 show the optical functions when the quadrupoles are placed at the same arc end (QD12.L5 and QD16.L5 respectively) with opposite strengths $(RL)_{SQ}/2 = \pm 9.1\,10^{-4}m^{-1}$. In particular the residual dispersion reaches about 0.32 m in the crossing triplet, less than 0.12 m in the others, and less than 0.05 m in the arcs.

Interlaced correction scheme

We extend the preceding consideration to an interlaced 4-pair assembly. The quadrupole correctors are installed next to the multipoles MSCBV in the LHC sequence at $D_x(s_{SQ})\sqrt{\beta_z(s_{SQ})} \approx 14.2$ (Table 9, column 3). The integrated correcting strength is matched with MAD with constraints exclusively on DY = 0 and DY' = 0 at IP and Octant ends The strength is essentially in the SQ1a/b.Left and SQ1a/b.Right pairs (Eq. 47 and column 5 of Table 9) ; their positioning coincides

Table 7: Optical functions at $IP1,2,5,8$ and other parameters obtained from a one-turn MAD TWISS procedure in presence of two skew quadrupole correctors placed at QD12.L5 and QD17.R5 with distinct strengths $(RL)_{SQ}|_{Left/Right}| \approx 10.6\,10^{-4}/-7.9\,10^{-4}m^{-1}$, prior to any additional re-tuning of the IR.

pos.	lmnt	beta1 beta2	alfa1 alfa2	mu1 mu2 [2pi]	R11 R21	R12 R22	xco yco [mm]	pxco pyco [.001]	Dx Dy	Dpx Dpy
1	IP1	0.501	0.000	0.000	0.039	0.015	0.000	0.000	0.000	0.000
		0.501	0.000	0.000	-0.105	0.029	0.000	0.000	0.000	0.000
599	IP2	0.500	-0.001	8.985	-0.021	-0.019	0.000	0.000	0.000	0.000
		0.501	-0.003	7.540	0.124	-0.014	0.000	0.000	0.000	0.000
2411	IP5	0.498	0.001	31.640	-0.021	0.043	0.000	0.000	0.000	0.000
		0.502	0.003	31.655	-0.078	0.034	0.000	0.100	-0.003	-0.003
4202	IP8	0.500	-0.001	55.745	-0.027	-0.020	0.000	0.000	0.000	0.000
		0.501	0.002	54.322	0.120	-0.013	0.000	0.000	0.000	0.000
Q1 = 63.280049						Q2 = 63.310209				
betax(max)= 4447.25488						betay(max) =4424.177009				
Dx(max) = 2.177816						Dy(max) = 0.203188				
yco(max) = 4.707107										

Table 8: Optical functions at $IP1,2,5,8$ and other parameters obtained from a one-turn MAD TWISS procedure in presence of two skew quadrupole correctors placed at the same end of the IR (next to QD12.L5 and QD16.L5 respectively) with opposite strengths, prior to any re-tuning of the IR.

pos.	lmnt	beta1 beta2	alfa1 alfa2	mu1 mu2 [2pi]	R11 R21	R12 R22	xco yco [mm]	pxco pyco [.001]	Dx Dy	Dpx Dpy
1	IP1	0.500	0.000	0.000	0.000	0.000	0.000	0.000	0.000	0.000
		0.500	0.001	0.000	0.000	0.000	0.000	0.000	0.002	0.000
599	IP2	0.500	0.000	8.985	0.000	0.000	0.000	0.000	0.000	0.000
		0.500	-0.003	7.540	-0.001	0.000	0.000	0.000	-0.002	0.001
2413	IP5	0.500	0.000	31.640	-0.001	0.000	0.000	0.000	0.000	0.000
		0.502	-0.001	31.655	-0.001	0.000	0.000	0.100	0.007	-0.004
4202	IP8	0.500	0.000	55.745	0.001	0.000	0.000	0.000	0.000	0.000
		0.500	0.003	54.322	0.000	0.000	0.000	0.000	0.002	-0.001
Q1 = 63.280015						Q2 = 63.310005				
betax(max)= 4431.614434						betay(max) =4430.117034				
Dx(max) = 2.177883						Dy(max) = 0.322977				
yco(max) = 4.707107										

Table 9: Corrector strengths necessary for canceling the chromatic bump opened in the left and right odd-type low-β triplets by the non-zero horizontal c.o. due to $z'^* = 10^{-4} rad$ c.o. angle at IP, as obtained from a MAD match. The correctors are all placed next to the lattice multipole correctors at high $D_x(s_{SQ})\sqrt{\beta_z(s_{SQ})}$ values (column 3). The pairs SQ1a/b.Left and SQ1a/b.Right are almost $\pi/\nu[\pi/\nu]$ distant from respectively the left- and right-hand side low-β triplets (column 4), they play the dominant role, with integrated strengths $|(RL)_{SQ}|_{Left/Right}| = 10.3\,10^{-4}/7.8\,10^{-4} m^{-1}$ [twice the value in column 5, consistent with Eq. (47)] ; the pairs SQ2a/b.Left and SQ2a/b.Right are almost $\pi/2\nu[\pi/\nu]$ distant from respectively the left- and right-hand side low-β triplets, and have weak role as expected (column 5).

Corrector name	Neighboring quadrupole	$D_x(s_{SQ})\sqrt{\beta_z(s_{SQ})}$ $(m^{3/2})$	Phase w.r.t. IP $(\pi/2\nu)$	$(KL)_{SQ}$ $(10^{-4}m^{-1})$
SQ2a/b.Left	QD12/16.Left	14.2	-1.779 / -2.281	± 1.07
SQ1a/b.Left	QT.Q10/14.Left	14.2	-1.528 / -2.030	± 5.15
SQ1a/b.Right	QD11/15.Right	14.2	1.019 / 1.521	± 3.90
SQ2a/b.Right	QD13/17.Right	14.2	1.269 / 1.771	± 0.52

Table 10: Optical functions at $IP1, 2, 5, 8$ and other parameters obtained from a one-turn MAD TWISS procedure in presence of interlaced four skew quadrupole corrector pairs tuned as shown in Table 9, prior to any additional re-tuning of the IR.

pos.	lmnt	beta1 beta2	alfa1 alfa2	mu1 mu2 [2pi]	xco yco [mm]	pxco pyco [.001]	Dx Dy	Dpx Dpy
1	$IP1$	0.500	0.000	0.000	0.000	0.000	0.000	0.000
		0.500	0.001	0.000	0.000	0.000	0.000	0.000
599	$IP2$	0.500	0.000	8.985	0.000	0.000	0.000	0.000
		0.500	-0.003	7.540	0.000	0.000	0.000	0.000
2417	$IP5$	0.500	0.000	31.640	0.000	0.000	0.000	0.000
		0.502	-0.001	31.655	0.000	0.100	0.000	0.000
4214	$IP8$	0.500	0.000	55.745	0.000	0.000	0.000	0.000
		0.500	0.004	54.322	0.000	0.000	0.000	0.000

Q1 = 63.280012	Q2 = 63.310003
betax(max)= 4431.547892	betay(max) = 4430.849387
Dx(max) = 2.178292	Dy(max) = 0.195784
Dx(r.m.s.) = 1.500096	Dy(r.m.s.) = 0.017911
xco(max) = 0.000001	y_{co}(max) = 4.707107

with almost $\pi/2\nu[\pi/\nu]$ distance from the IP, on respectively the left- and right-hand side of the IR (by QD10/14.Left and QD11/15.Right). The weak role of SQ2a/b.Left and SQ2a/b.Right companion pairs (distant almost $\pi/\nu[\pi/\nu]$ from the IP, on respectively the left- and right-hand side of the IR, by QD12/16.Left and QD13/17.Right) is shown in Table 9 (column 5) ; they however do help canceling residual perturbative dispersion.

The residual dispersion in the arcs is quasi-zero (Fig. 17). The absence of effect on the first order focusing is apparent in Table 10 which displays the ensuing values of the optical functions at $IP1, 2, 5, 8$, as well as tunes and other parameters as obtained from a one-turn MAD TWISS procedure without any additional re-tuning of the IR ; it is clear that any induced mismatch is negligible. Horizontal and vertical β-beating in the arcs are also negligible, and the machine tunes are not affected.

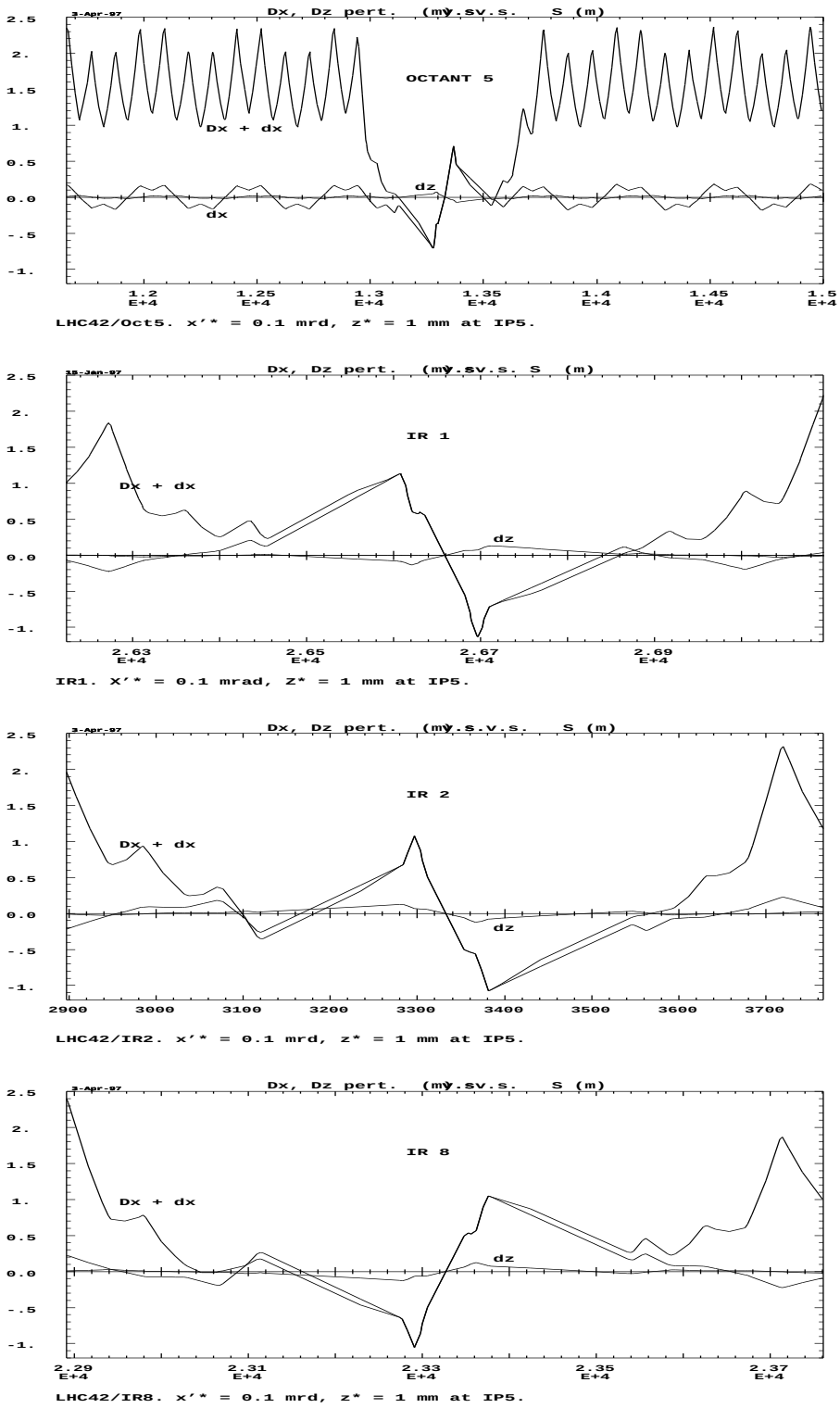

Figure 1: Horizontal (D_x, first order ; d_x, perturbative), and vertical (d_z, perturbative) closed dispersions (Eq. 10), under the effect of respectively $x'^* = 10^{-4} rad$ horizontal c.o. angle and $z'^* = 10^{-3} m$ vertical c.o. off-centering at $IP5$, as observed at Octant 5, IR1, IR2 and IR8. As for the horizontal dispersion the upper left plot reveals about $\pm 10\%$ amplitude modulation in the arcs ; peak values of the dispersion at low-β triplets and derivatives at IP's are as stated in section 3.1 (Eqs. 26,28).

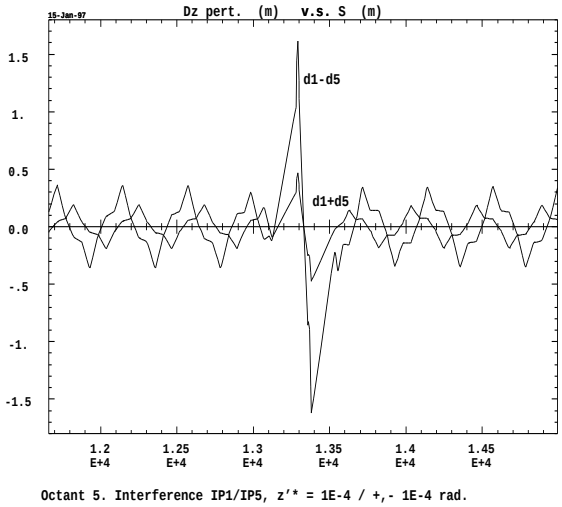

Figure 2: Building up of two-IP interference at Octant 5. Vertical c.o. angles are $z'^*(IP1) = 10^{-4} rad$ and $z'^*(IP5) = \pm 10^{-4} rad$. ${}^1d_z(s)$ and ${}^5d_x(s)$ are the independent closed solutions of Eq. (8) obtained under single crossing at respectively $IP1$ and $IP5$ ("d_X" plots in Fig. 1). The sum interference ${}^1d_z(s) + {}^5d_z(s)$ is obtained with identical c.o. angle signs at $IP5$ and $IP1$; the difference interference ${}^1d_z(s) - {}^5d_z(s)$ brings up to 1.63 m peak dispersion in the low-β triplets. Note that, since the two perturbations are not excited in phase there is not full cancellation (neither full addition) of amplitudes.

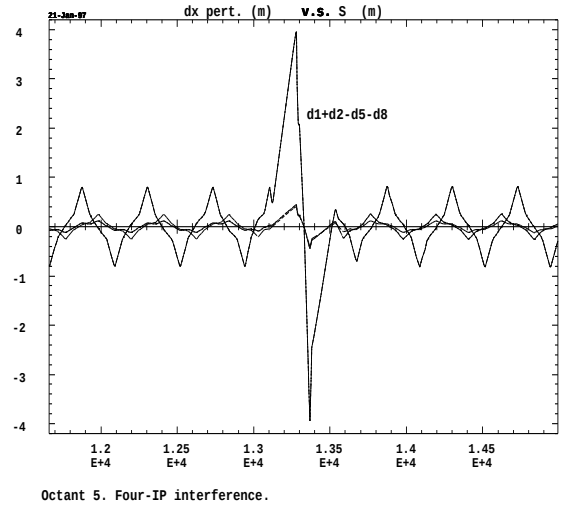

Figure 3: Four-IP interference as observed at Octant 5. All crossings are in the horizontal plane, $x'^* = \epsilon_{IP} 10^{-4} rad$, with $\epsilon_1 = \epsilon_2 = \epsilon_5 = \epsilon_8 = 1, \epsilon_1 = \epsilon_2 = 1$ and $\epsilon_5 = \epsilon_8 = -1, \epsilon_1 = \epsilon_5 = 1$ and $\epsilon_2 = \epsilon_8 = -1$.

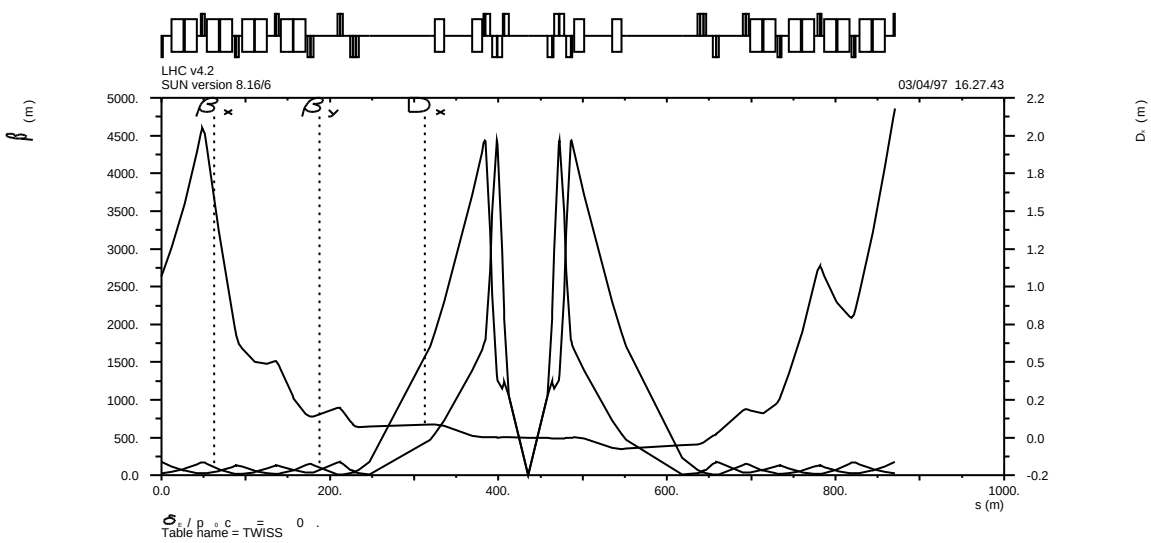

Figure 4: Betatron and second order dispersion functions across IR5 in presence of $x'^* = 10^{-4} rad$ horizontal c.o. angle, after compensation of the horizontal anomalous dispersion by mere re-tuning of the IR ; the only noticeable (though negligible) difference w.r.t. regular optics is the non-zero dispersion in the low-β triplets.

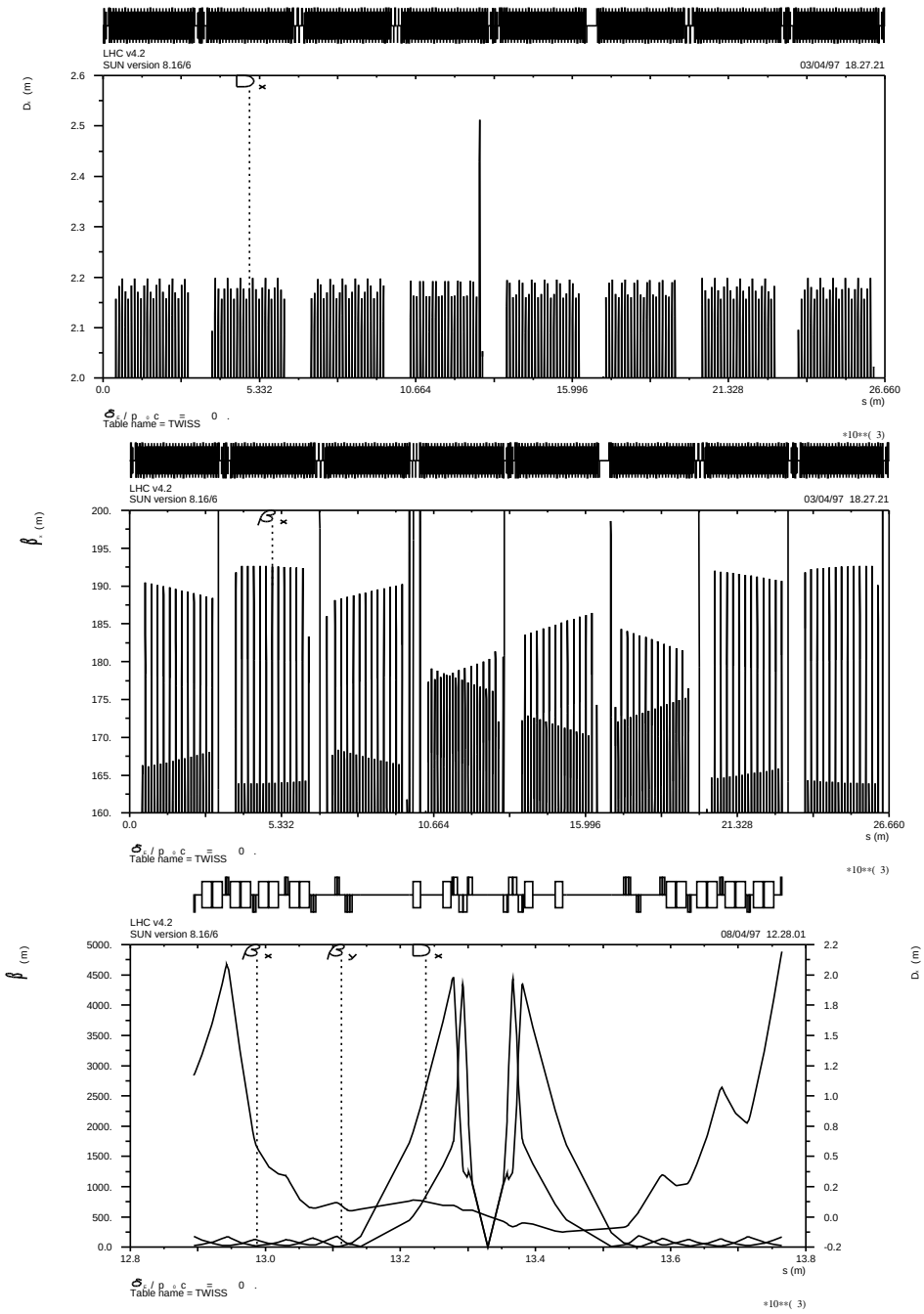

Figure 5: Single quadrupole compensation of the anomalous dispersion induced by $10^{-4} rad$ horizontal c.o. angle at $IP5$. The quadrupole is placed at QF13.Left at the left end of IR5, with strength $(KL)_q = -9.1\,10^{-4} m^{-1}$ (after Eq. 38). There is no additional re-tuning of the IR. *Upper plot* : extrema of the dispersion function, it can be observed that the residual modulation is very small (1%). *Middle* : horizontal β-beating, the modulation is about 8.5% (the quadrupole has similar though much smaller effect in the vertical plane, inducing about 1.5% modulation, not shown here) ; *lower plot* : general shape of the optical functions at IR5 ; it can be observed that the d_x peak in the low-β triplet is strongly decreased, from 0.71 m (Eq. 26 and Fig. 1) down to about 0.08 m ; the dispersion and derivative at IP5 are $D_x \approx 10\,10^{-3} m$, $D'_x \approx -2\,10^{-3} rad$ and respectively less than $10^{-3} m$, $5\,10^{-4} rad$ at other collision IP's.

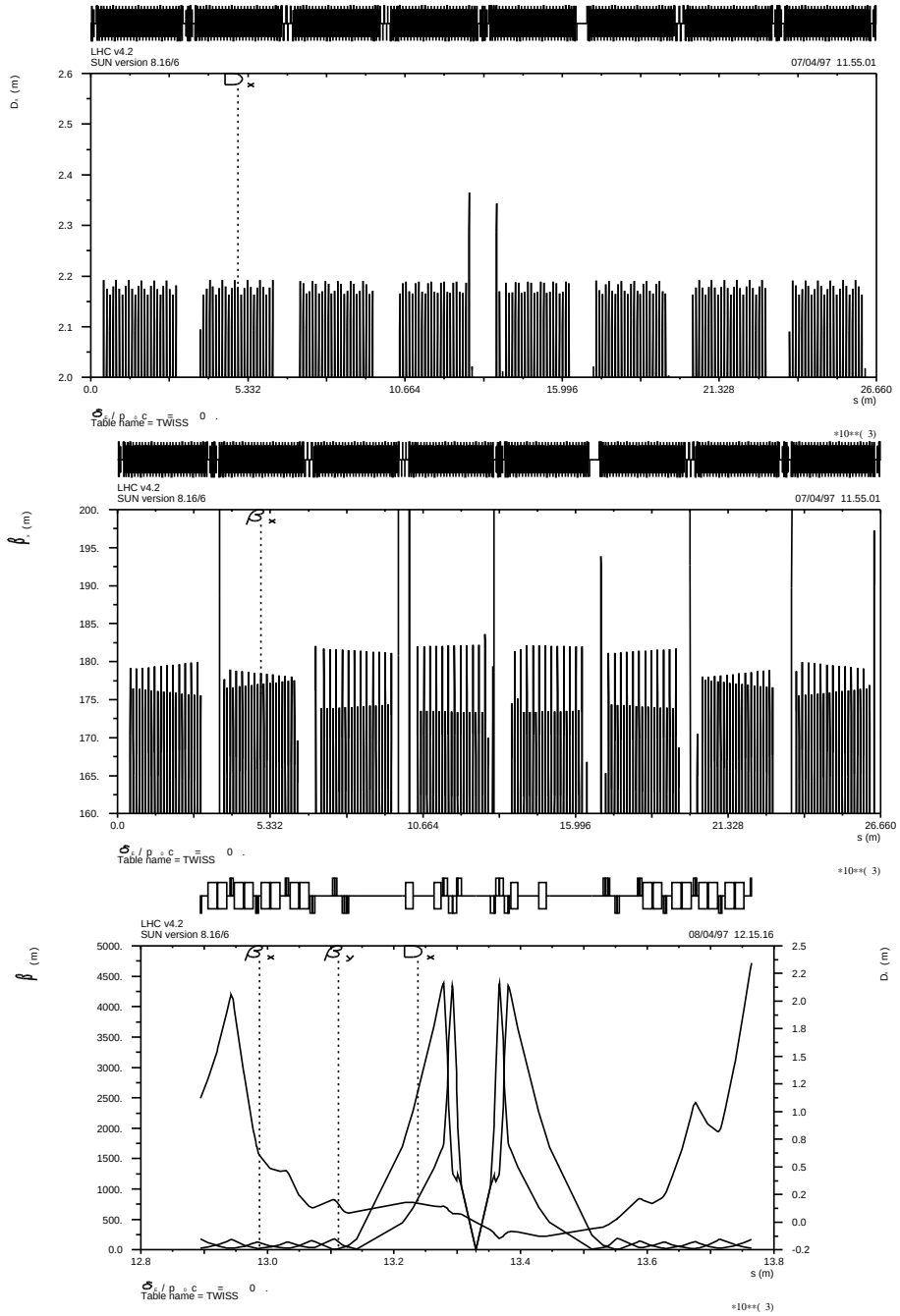

Figure 6: Double quadrupole compensation of the anomalous dispersion induced by $10^{-4} rad$ horizontal c.o. angle at $IP5$. The quadrupoles are placed at opposing arc ends respectively by QF13.Left at the left end and QF16.Right at the right end of IR5 with respectively half the strength $(KL)_Q = \mp 9.1\, 10^{-4}/2\, m^{-1}$ (after Eq. 38). There is no additional re-tuning of the IR. *Upper plot* : extrema of the dispersion function, comparable to the single quadrupole case ($\approx 1\%$ residual modulation). *Middle* : horizontal β-beating, the modulation is about 1.5%, strongly improved w.r.t. Fig. (5) (and much less than 1% in the vertical plane, not shown here) ; *lower plot* : general shape of the optical functions at IR5 ; the dispersion and derivative at IP5 are $D_x \approx 2\, 10^{-3} m$, $D'_x \approx -3\, 10^{-3} rad$, and respectively less than $10^{-3} m$, $510^{-4} rad$ at other collision IP's.

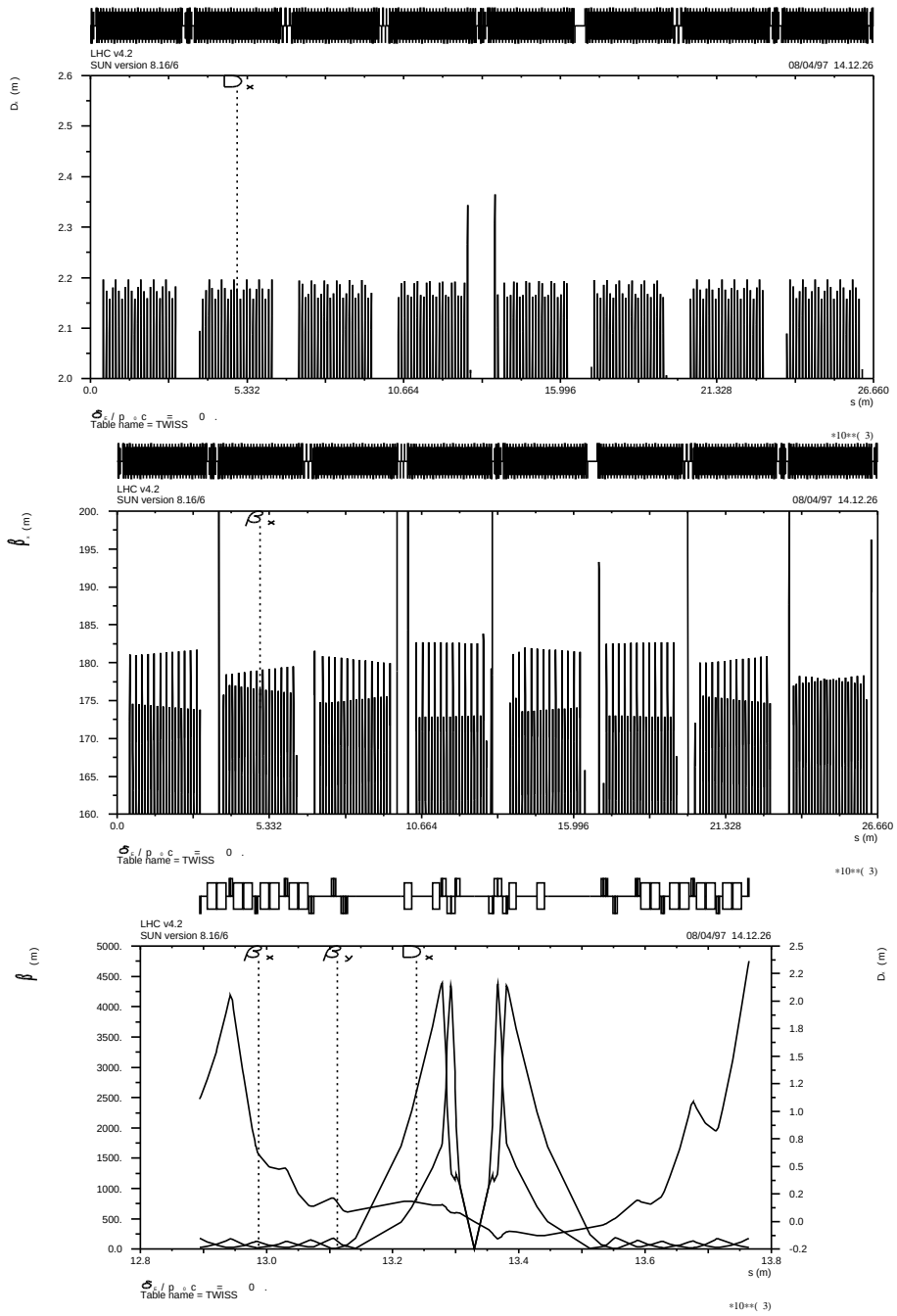

Figure 7: Double quadrupole compensation of the anomalous dispersion induced by $10^{-4} rad$ horizontal c.o. angle at *IP*5. The quadrupoles are placed at opposing arc ends respectively by QF13.Left at the left end and QF16.Right at the right end of IR5 with *distinct* respective strengths $(KL)_Q = -3.9\,10^{-4}\,m^{-1}$, $(KL)_Q = +5.2\,10^{-4}\,m^{-1}$ balancing each one the corresponding low-β triplet (after Eq. 38). There is no additional re-tuning of the IR. *Upper plot* : extrema of the dispersion function, comparable to the single quadrupole case ($\approx 1\%$ residual modulation). *Middle* : horizontal β-beating, the modulation is about 1.5%, strongly improved w.r.t. Fig. (5) (and much less than 1% in the vertical plane, not shown here) ; *lower plot* : general shape of the optical functions at IR5 ; the dispersion and derivative at IP5 are $D_x \approx 10^{-3} m$, $D'_x \approx -3\,10^{-3} rad$, and respectively less than $10^{-3} m$, $5\,10^{-4} rad$ at other collision IP's.

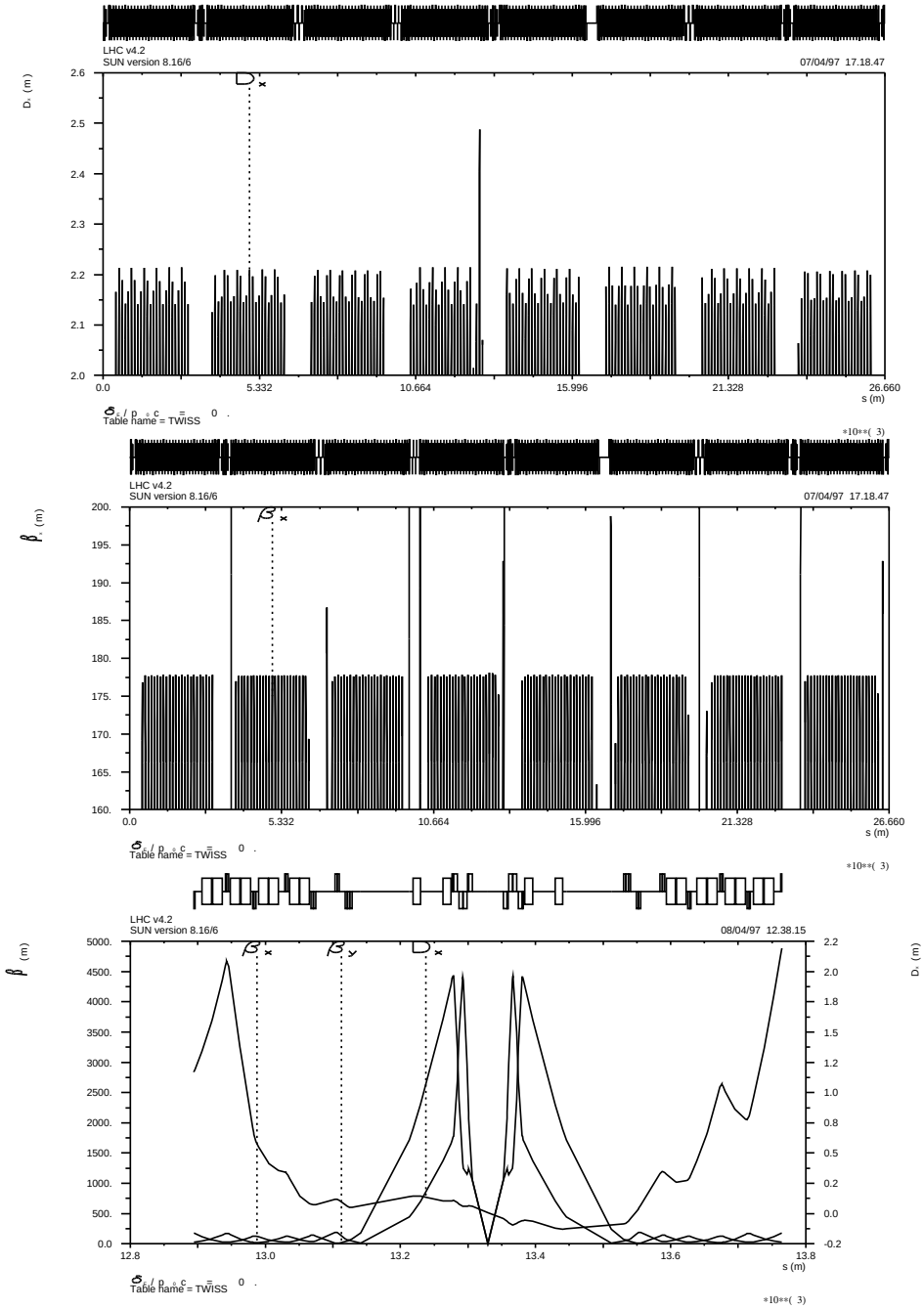

Figure 8: Double quadrupole compensation of the anomalous dispersion induced by $10^{-4} rad$ horizontal c.o. angle at $IP5$. The two quadrupoles are placed at the same end of IR5, respectively by QF13.Left and QF17.Left with strengths $(KL)_q \approx \mp 9.1\,10^{-4}/2\ m^{-1}$. There is no additional re-tuning of the IR. *Upper plot* : extrema of the dispersion function, comparable to the single quadrupole case. *Middle* : horizontal β-beating, the modulation is negligible, strongly improved w.r.t. Fig(5.3) (and much less than 1% in the vertical plane, not shown here) ; *lower plot* : general shape of the optical functions at IR5 ; the dispersion and derivative at IP5 are $D_x \approx 2\,10^{-3} m$, $D'_x \approx -2\,10^{-3} rad$, and respectively less than $10^{-3} m$, $5\,10^{-4} rad$ at other collision IP's.

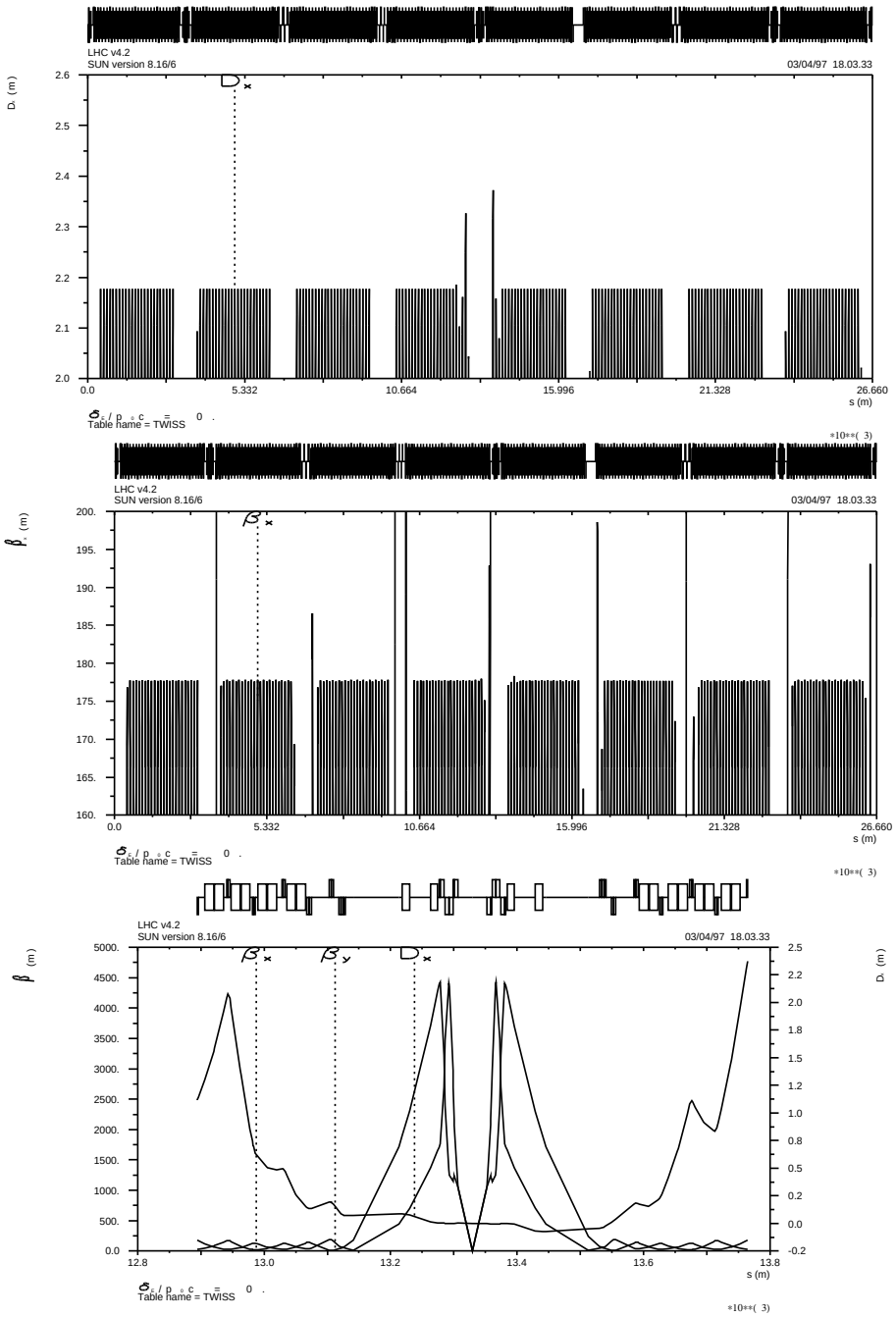

Figure 9: Compensation of the horizontal anomalous dispersion due to $x'^* = 10^{-4} rad$ c.o. angle at $IP5$, with four quadrupole pairs placed at the arcs ends (Tables 3,4). *Upper plot* : peak amplitudes of the dispersion along the ring ; no noticeable modulation remains. Only local modulation within the dispersion bump in IR5 is left. *Middle plot* : peak amplitudes of the beta functions in the arcs along the ring. The horizontal and vertical β-beating are respectively $\pm 0.15\%$ and $\pm 0.5\%$. *Lower plot* : general shape of the optical functions at IR5.

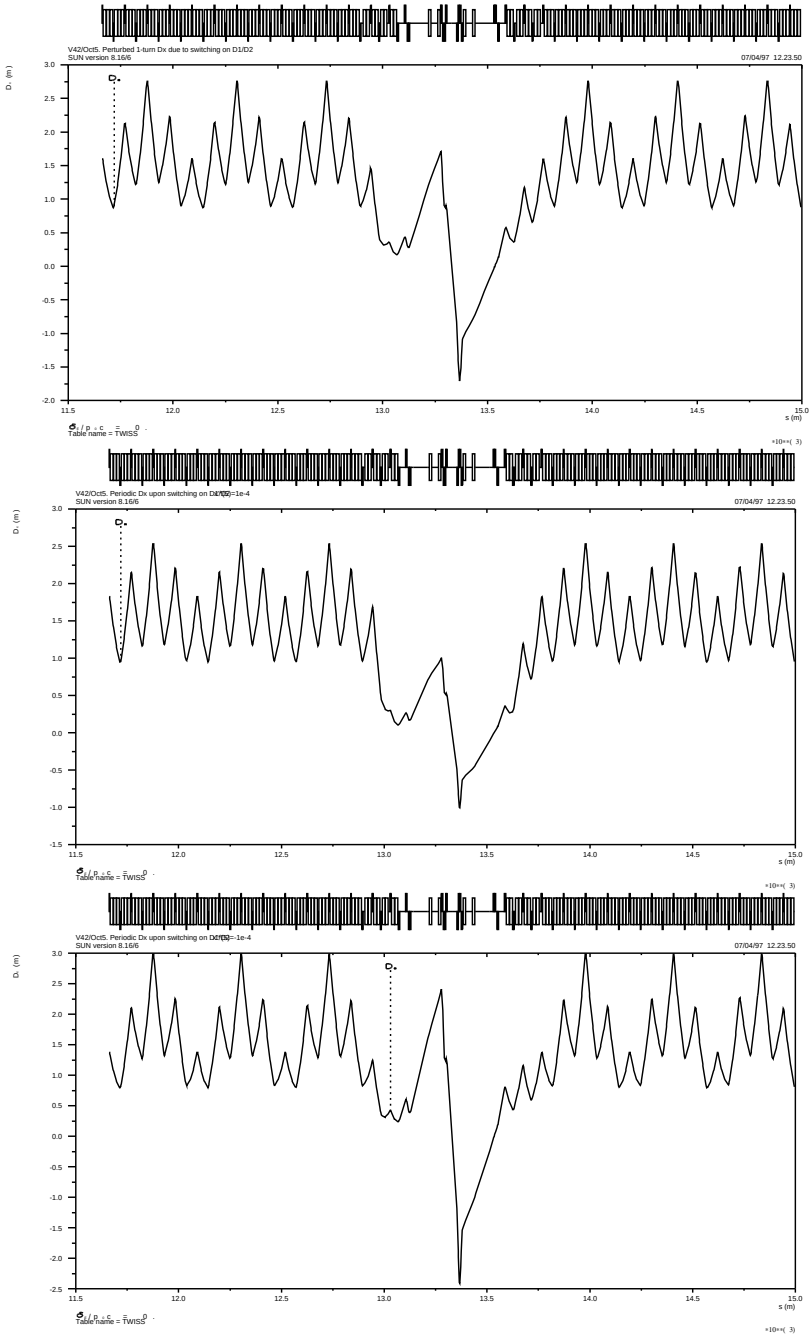

Figure 10: *Upper plot* : first order dispersion function as perturbed by switching on the D1/D2 separator/recombiner dipole pairs while the IR has been tuned beforehand with D1/D2 pairs off ; the extremum value of D_x is 2.76 m [namely, the regular extremum 2.178 m increased by the modulation of 0.6 m (Eq.20)], reached in the arcs. *Middle plot* : second order dispersion function $D_x + d_x$ under the effect of the anomalous dispersion induced by $x'^* = 10^{-4} rad$ horizontal c.o. angle at the IP ; w.r.t. the upper plot the extremum value in the arcs has been damped by about 35% (Eqs. 2) down to 2.58 m. *Lower plot* : second order dispersion function $D_x + d_x$ under the effect of the anomalous dispersion induced by $x'^* = -10^{-4} rad$ horizontal c.o. angle at the IP ; w.r.t. the upper plot the extremum value in the arcs has been increased by about 35% up to 3 m

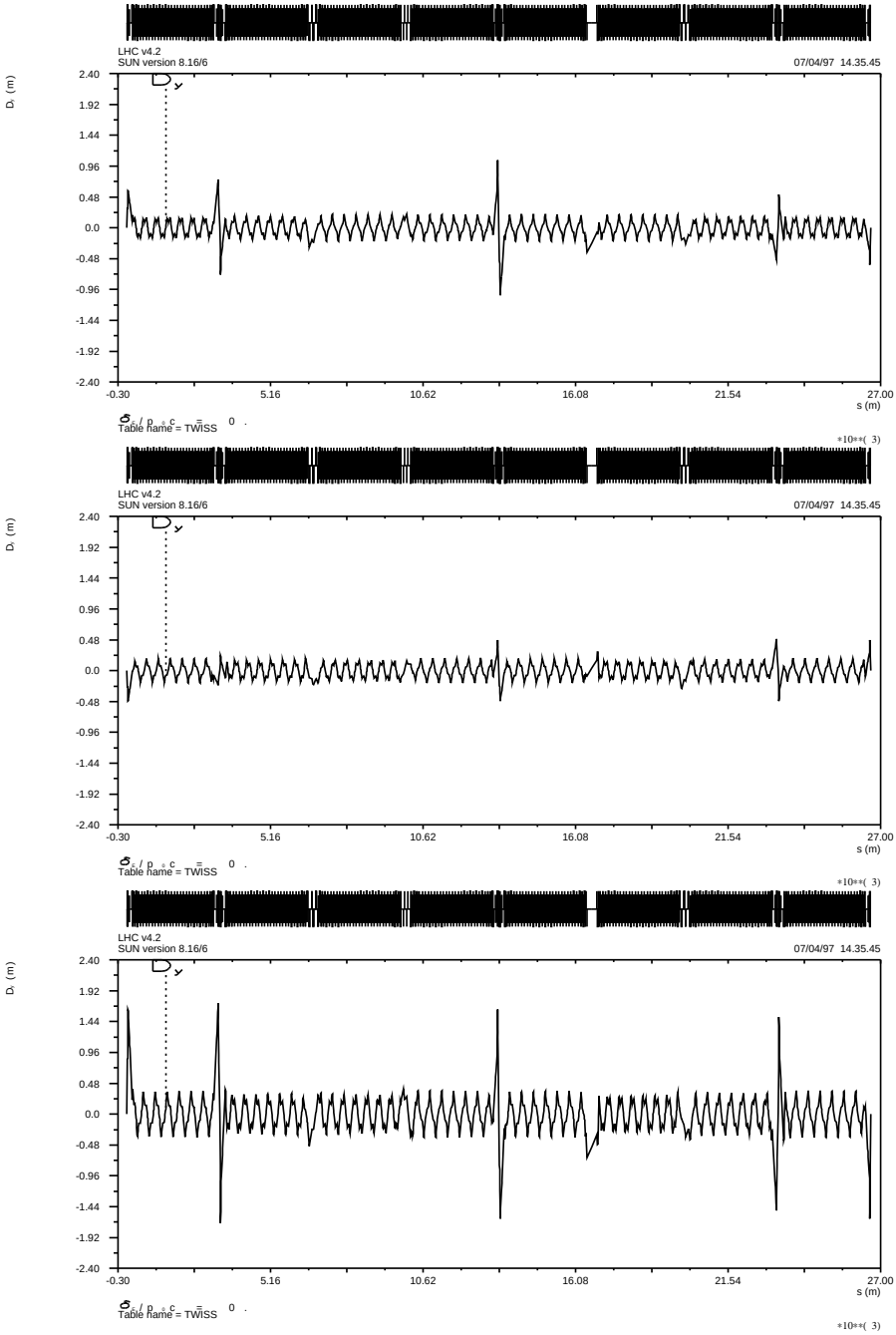

Figure 11: Vertical interference between $IP1$ and $IP5$ (these simulations are identical to the results displayed in Fig. 2). *Upper plot* : second order dispersion function $D_x + d_x$ along the ring under single $10^{-4} rad$ vertical c.o. angle at IP1. *Middle* :$10^{-4} rad$ c.o. angle at $IP1$ and $10^{-4} rad$ at $IP5$. *Lower plot* : $10^{-4} rad$ at $IP1$ and $-10^{-4} rad$ at $IP5$.

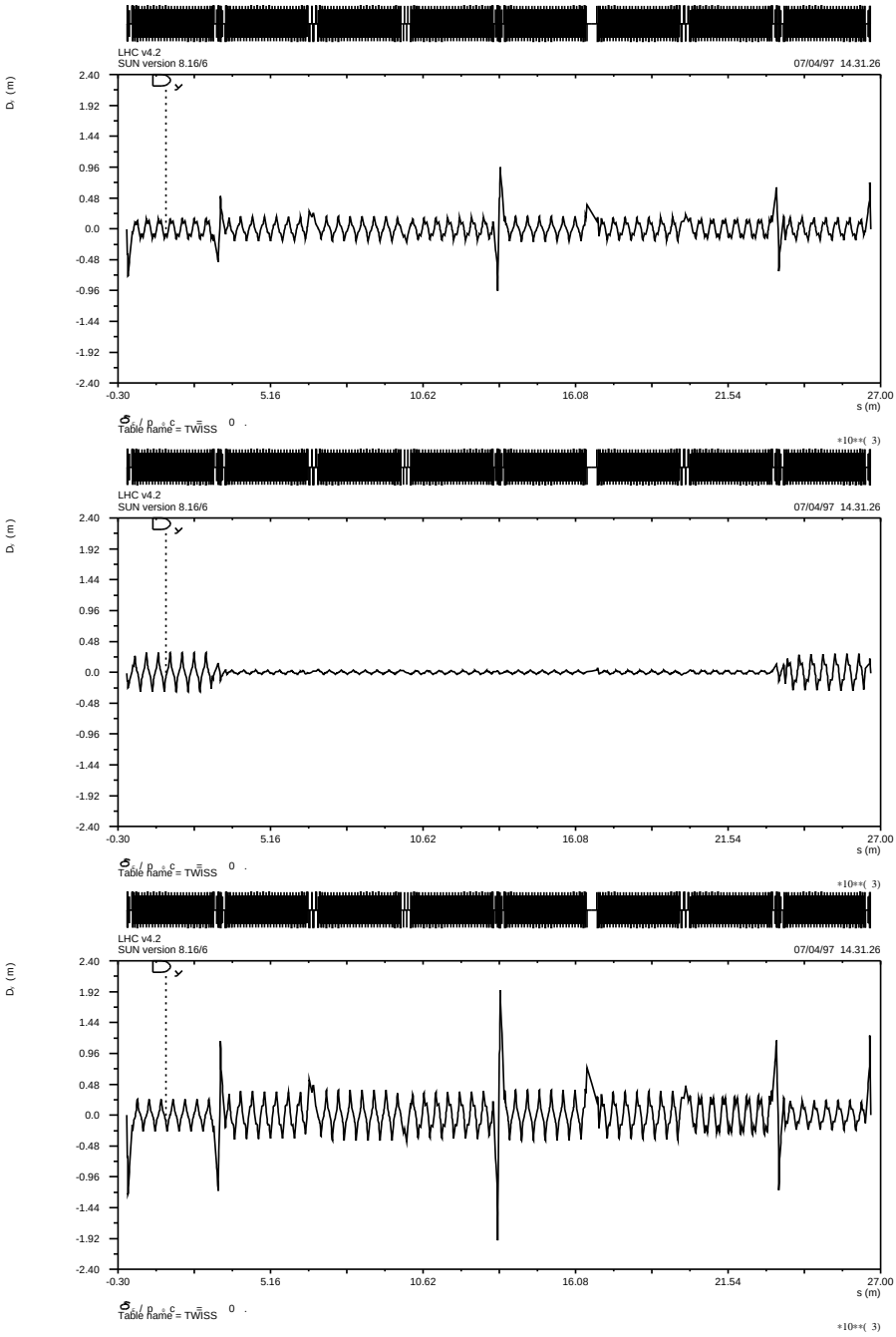

Figure 12: Vertical interference between $IP2$ and $IP8$. *Upper plot* : second order dispersion function d_z along the ring under single $10^{-4} rad$ vertical c.o. angle at $IP2$; peak amplitude $\bar{d}_z = 0.96\,m$ in $IP5$ low-β triplet. *Middle* : $10^{-4} rad$ c.o. angle at $IP2$ and $10^{-4} rad$ at $IP8$; maximum amplitude $\bar{d}_z = 0.24\,m$ in the range ARC8/ARC1. *Lower plot* : $10^{-4} rad$ at $IP2$ and $-10^{-4} rad$ at $IP8$; peak amplitude $\bar{d}_z = 1.95\,m$ in $IP5$ low-β triplet.

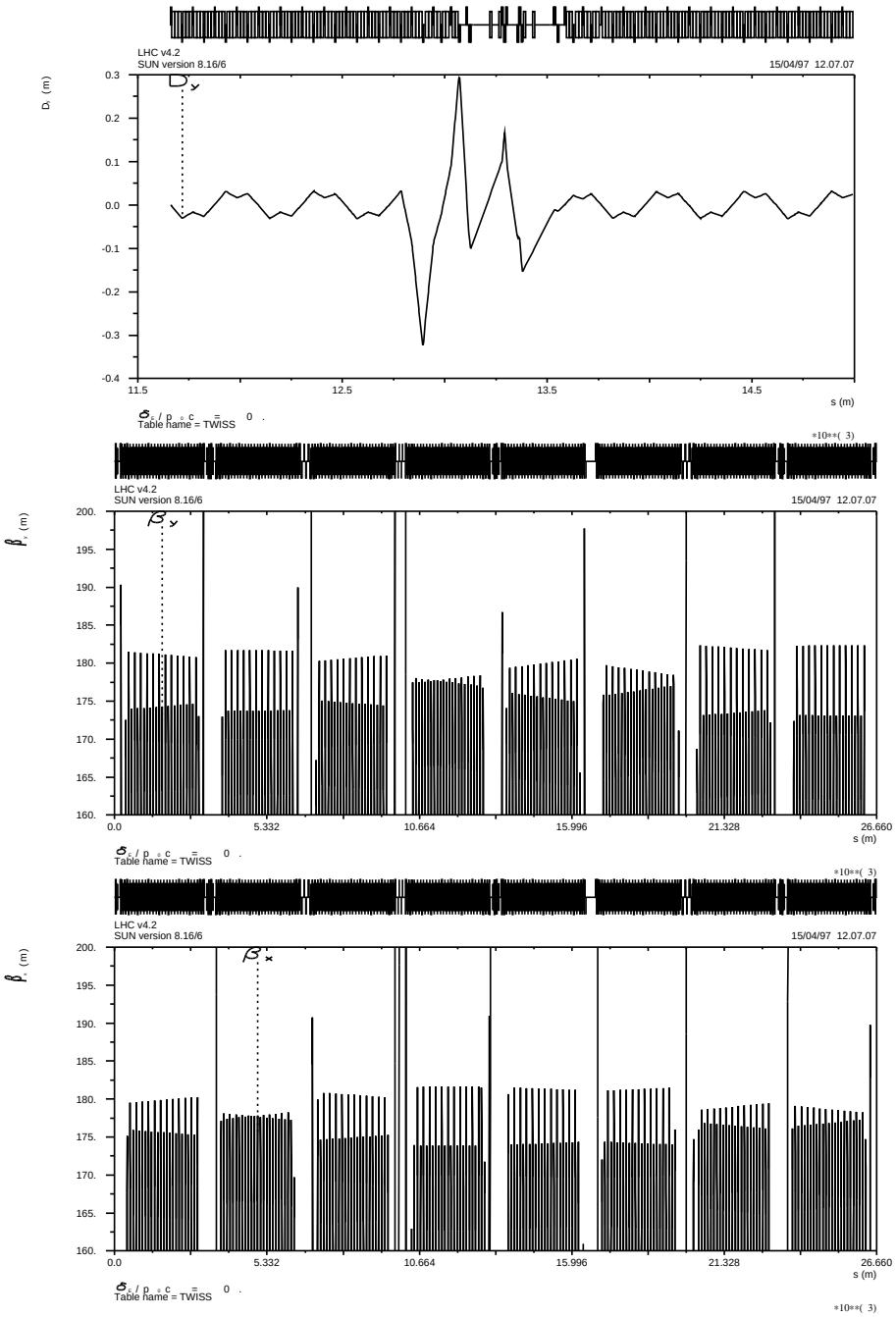

Figure 13: Compensation of the vertical anomalous dispersion due to $z'^{*} = 10^{-4} rad$ c.o. angle at $IP5$, with one skew quadrupole placed at QD12.L5. Upper plot : residual dispersion at Octant 5. Middle plot : peak amplitudes of the horizontal β function along the ring.Lower plot : peak amplitudes of the vertical β function along the ring.

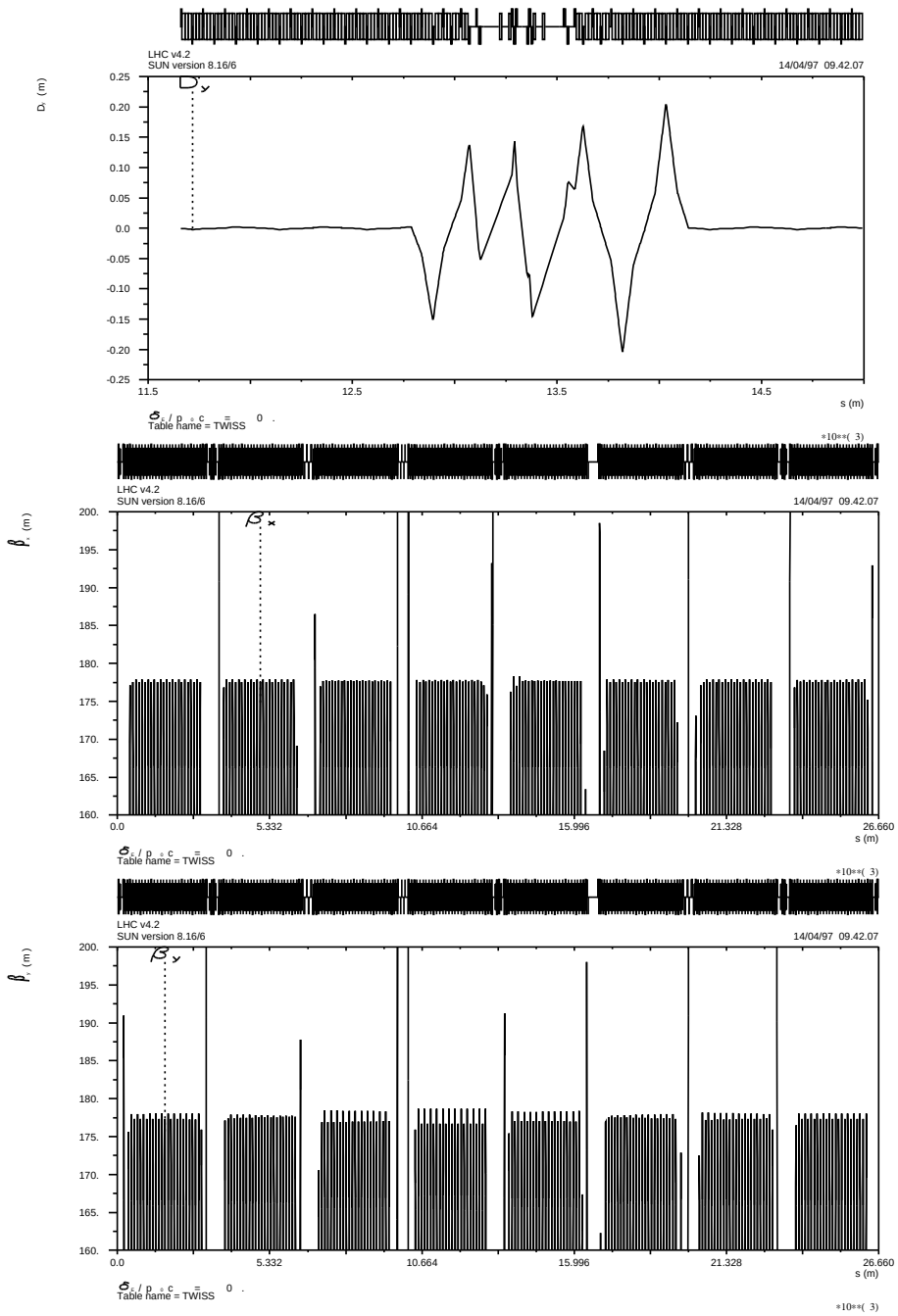

Figure 14: Compensation of the vertical anomalous dispersion due to $z'^{*} = 10^{-4} rad$ c.o. angle at $IP5$, with two skew quadrupoles placed one at each arc end (QD12.L5 and QD17.R5 respectively) with opposite strengths $(RL)_{SQ}/2 = \pm 9.1\, 10^{-4} m^{-1}$. Upper plot : residual dispersion at Octant 5. Middle plot : peak amplitudes of the horizontal β function along the ring. Lower plot : peak amplitudes of the vertical β function along the ring.

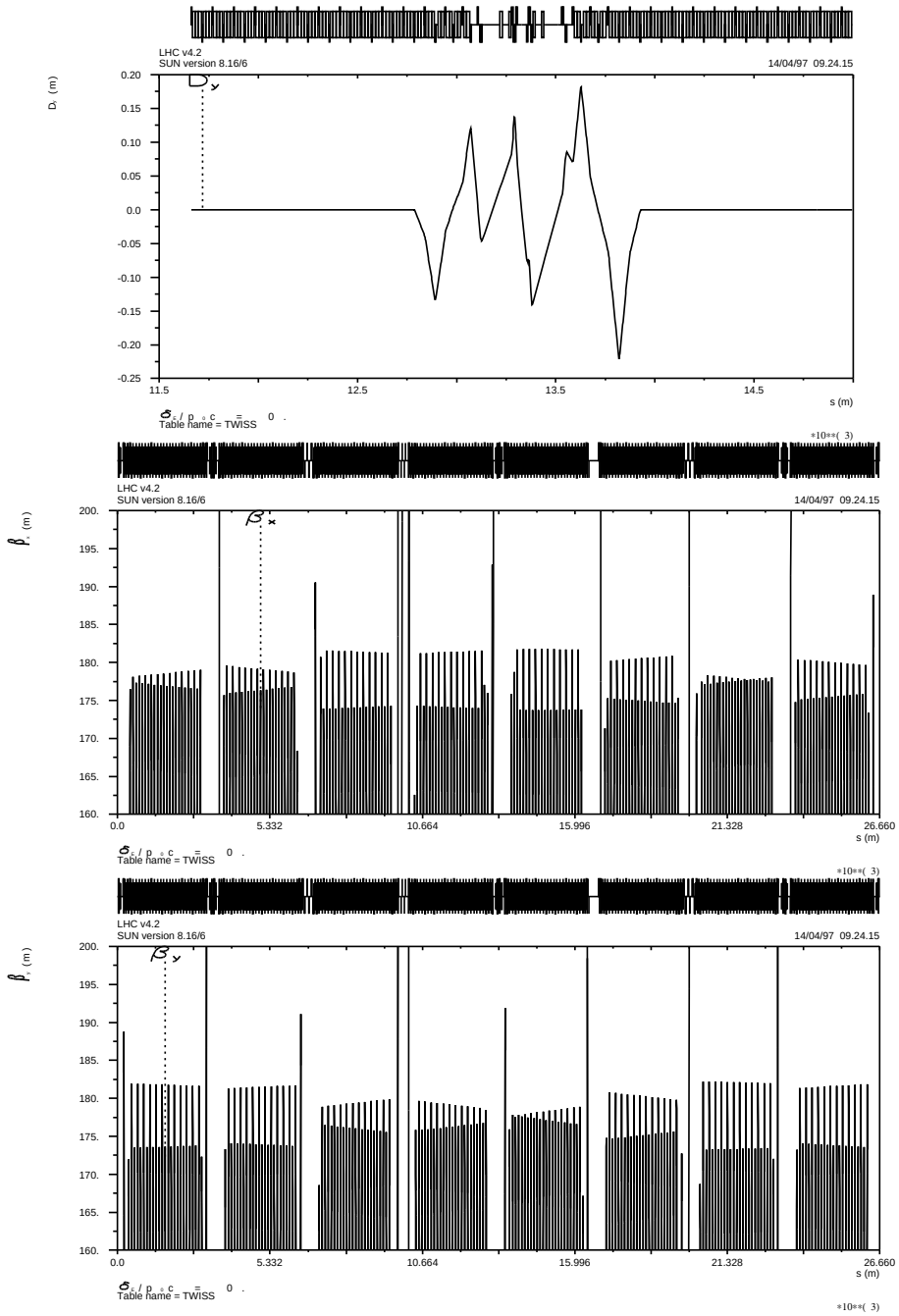

Figure 15: Compensation of the vertical anomalous dispersion due to $z'^{*} = 10^{-4} rad$ c.o. angle at $IP5$, with two skew quadrupoles placed one at each arc end (QD12.L5 and QD17.R5 respectively) with distinct strengths $(RL)_{SQ}|_{Left/Right}| \approx 10.6\,10^{-4}/-7.9\,10^{-4} m^{-1}$ balancing the respective strength of the opposite low-β triplet. Upper plot : residual dispersion at Octant 5. Middle plot : peak amplitudes of the horizontal β function along the ring. Lower plot : peak amplitudes of the vertical β function along the ring.

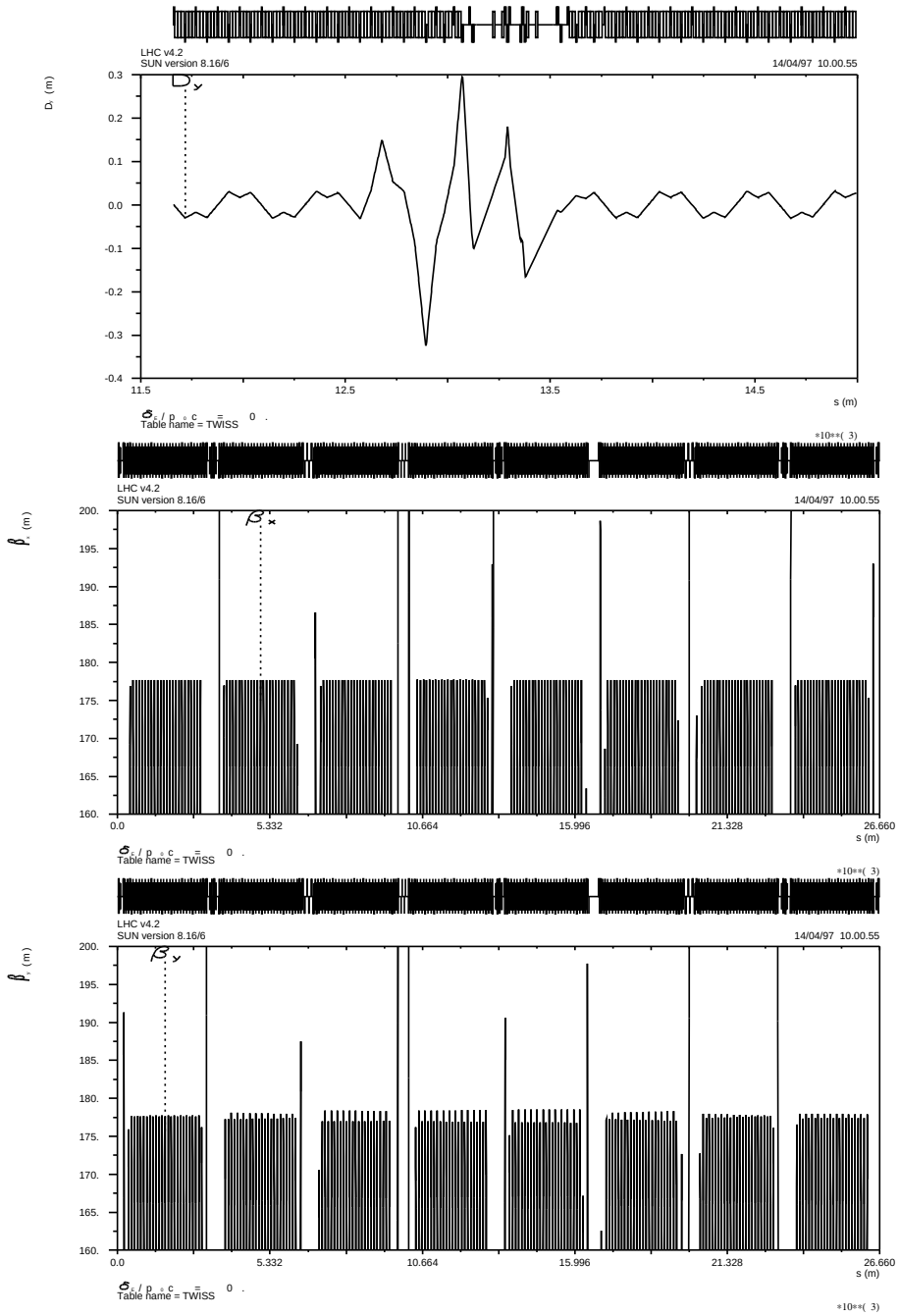

Figure 16: Compensation of the vertical anomalous dispersion due to $z'^{*} = 10^{-4} rad$ c.o. angle at $IP5$, with two skew quadrupoles placed at the same arc end (QD12.L5 and QD16.L5 respectively) with opposite strengths $(RL)_{SQ}/2 = \pm 9.1\,10^{-4} m^{-1}$. Upper plot : residual dispersion at Octant 5 ; it is comparable to the single quadrupole case (Fig. 13) remains. Middle plot : peak amplitudes of the horizontal β function along the ring. Lower plot : peak amplitudes of the vertical β function along the ring.

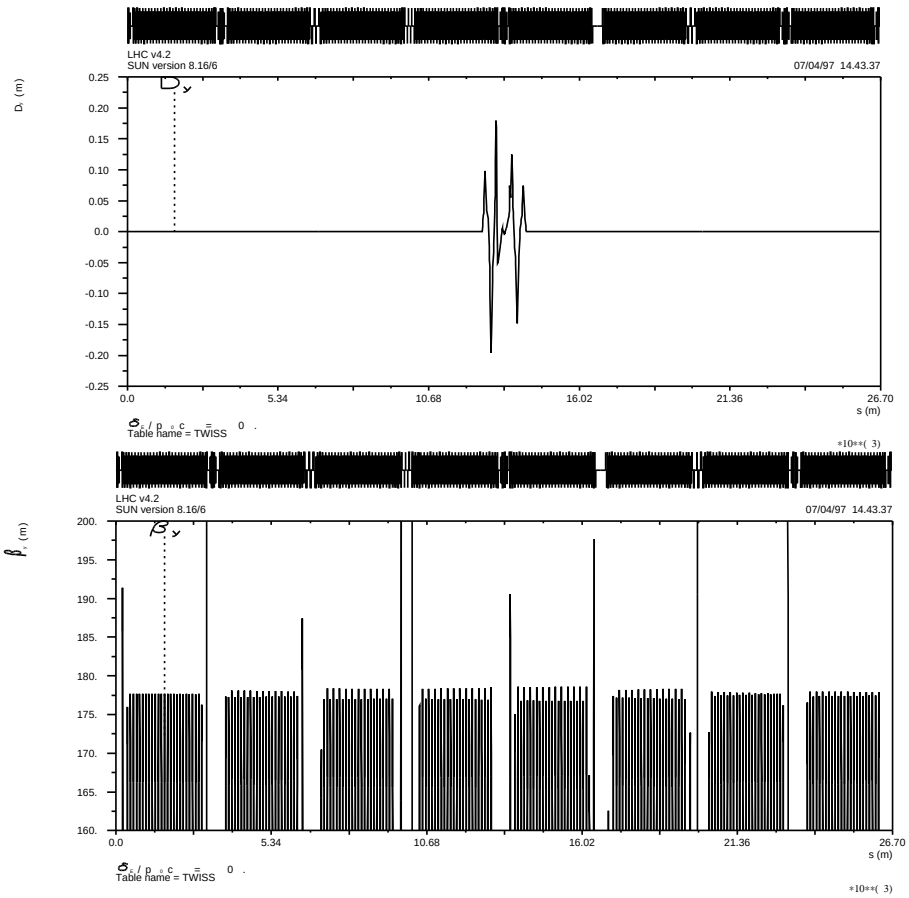

Figure 17: Compensation of the vertical anomalous dispersion due to $z'^{*} = 10^{-4} rad$ c.o. angle at $IP5$, with four skew quadrupole pairs placed at the arcs ends (Tables 9,10). Upper plot : residual dispersion along the ring ; it is practically zero outside the IR. Lower plot : peak amplitudes of the vertical β functions in the arcs along the ring.

A Appendix : Beam crossing and off-centering schemes

- LHC 4.2 optics -

Appendix A describes the crossing and/or off-centering closed orbit (c.o.) bumps on which the numerical applications and other plots presented in this report are based.

A priori, adequate phase shift w.r.t. the IP, in collision mode where it is the most critical, should be a strong criterion for the positioning of the c.o. dipoles (COD), in order to minimize the field strengths. However other criteria should be envisaged, such as

- the steering is possibly to include a combination of crossing or off-centering at IP in each plane (e.g., in order to achieve $\pm 45\,deg.$ inclined crossing plane). This imposes a pair of COD's per plane on each side of the IP (rather than a single one at π/ν (normalized) phase-shift in crossing optics, for instance),

- it may be desirable for aperture considerations to avoid additional non-zero c.o. in the outer triplet or dispersion suppressor magnets. For instance, on the left-hand side of odd-IP, π/ν phase-shift is attained at Q7.Left in LHC Version 4.2 optics ; a (single) steering dipole placed there to get $x'^* = 10^{-4} rad$ c.o. angle at the IP would produce $0.8\,10^{-3} m$ c.o. in Q5.Left.

This last criterion guided the present design in confining the c.o. bump within the range Q4A.L/Q4A.R. On each side of the IP, the horizontal and vertical COD pairs have been placed between the outer triplet and the separator/recombiner dipole D2 (Fig. 18). Typical strengths necessary to achieve $10^{-4} rad$ horizontal c.o. angle or $10^{-3} m$ vertical c.o. off-centering are given in Table 11.

Table 11: Dipole strengths for beam crossing/off-centering at IR1/5, collision optics.

	Horizontal c.o. angle $x'^* = 10^{-4} rad$	Vertical c.o. off-centering $z^* = 10^{-3} m$
K2L	-4.072315E-05	-2.630684E-05
K1L	1.319483E-05	6.466302E-05
K1R	2.126390E-11	4.055659E-05
K2R	2.248126E-05	-1.721094E-05

B Appendix : Sums related to the elementary kick model

- LHC 4.2 optics -

The following sums are obtained from MAD TWISS output, by means of a program derived from RDTWISS [12].

Sums relative to section 2 of the text.

$x'^* = 10^{-4} rad$ c.o. angle (half beam-beam horizontal angle), odd-type IP, collision optics

$\sum (KL)_q x_{co}(s_q) \sqrt{\beta(s_q)} \cos \nu[\pi + \phi(s_q)] = -2.573\,10^{-2}$,
$\sum (KL)_q x_{co}(s_q) \sqrt{\beta(s_q)} \sin \nu[\pi + \phi(s_q)] = -4.741\,10^{-3}$

$x^* = 10^{-3} m$ c.o. off-centering (half beam-beam horizontal distance at IP), odd-type IP, collision optics
$\sum (KL)_q x_{co}(s_q) \sqrt{\beta(s_q)} \cos \nu[\pi + \phi(s_q)] = -3.262\,10^{-3}$,
$\sum (KL)_q x_{co}(s_q) \sqrt{\beta(s_q)} \sin \nu[\pi + \phi(s_q)] = -5.290\,10^{-4}$

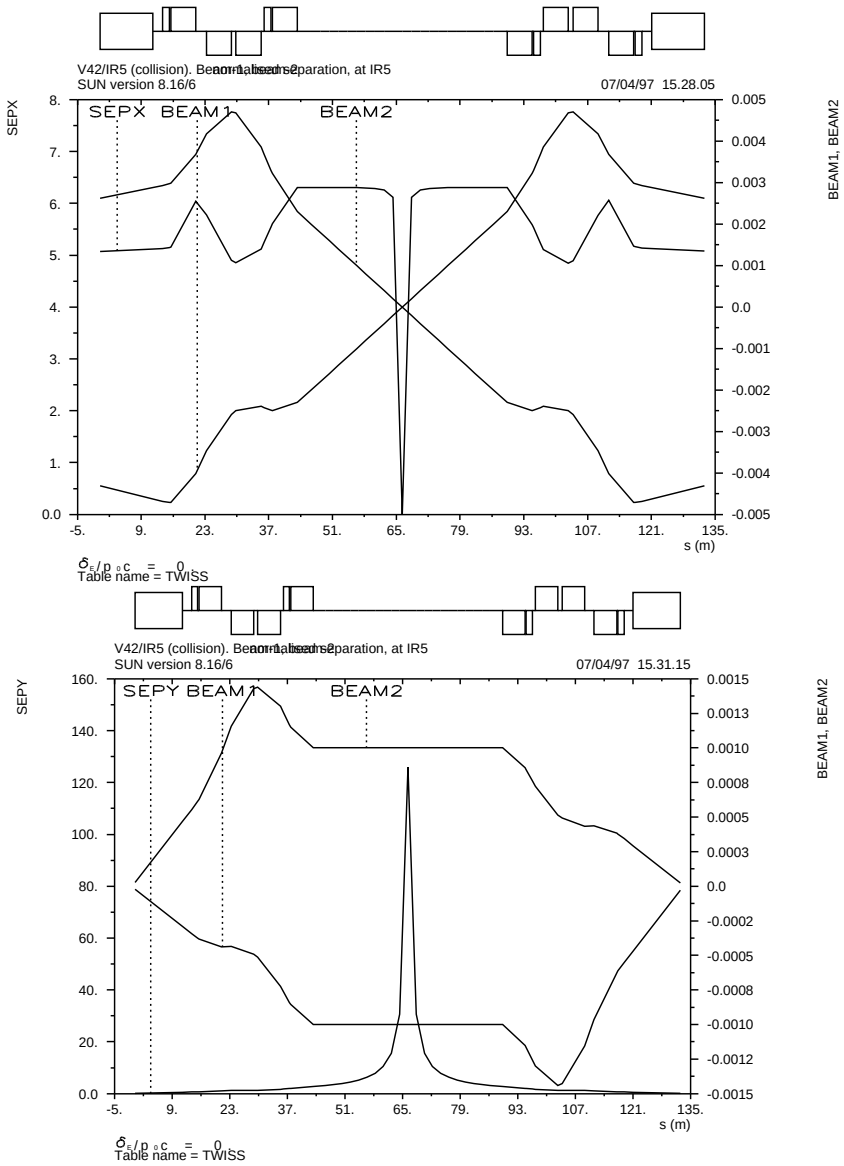

Figure 18: Collision optics. Horizontal $\pm 10^{-4} rad$ c.o. angle (top plot) and vertical $\pm 10^{-3} m$ off-centering (bottom plot). In both cases the beam-beam separation is normalized to largest σ-value. These geometries are used for numerical applications presented in the report.

$z^* = 10^{-3}m$ c.o. off-centering, odd-type IP, collision optics
$\sum(KL)_q z_{co}(s_q)\sqrt{\beta(s_q)}\cos\nu[\pi+\phi(s_q)] = 3.034\,10^{-3}$,
$\sum(KL)_q z_{co}(s_q)\sqrt{\beta(s_q)}\sin\nu[\pi+\phi(s_q)] = 1.302\,10^{-3}$

$z'^* = 10^{-4}rad$ c.o. angle, odd-type IP, collision optics
$\sum(KL)_q z_{co}(s_q)\sqrt{\beta(s_q)}\cos\nu[\pi+\phi(s_q)] = -2.421\,10^{-2}$,
$\sum(KL)_q z_{co}(s_q)\sqrt{\beta(s_q)}\sin\nu[\pi+\phi(s_q)] = -9.780\,10^{-3}$

Sums relative to section 5.2 of the text ($x'^* = 10^{-4}rad$ c.o. angle, collision optics, odd-type IR)

Left triplet : $\sum(KL)_{q_L} x_{co}(s_{q_L})\beta_x(s_{q_L}) = -1.12\,10^{-2}$
Right triplet : $\sum(KL)_{q_R} x_{co}(s_{q_R})\beta_x(s_{q_R}) = 1.50\,10^{-2}$

and, by antisymmetry, section 5.4 of the text ($z'^* = 10^{-4}rad$ c.o. angle, collision optics, odd-type IR)

Left triplet : $\sum(KL)_{q_L} z_{co}(s_{q_L})\sqrt{\beta_z(s_{q_L})} = -1.50\,10^{-2}$
Right triplet : $\sum(KL)_{q_R} z_{co}(s_{q_R})\sqrt{\beta_z(s_{q_R})} = 1.12\,10^{-2}$

Sums relative to section 3.1 of the text (crossing scheme, horizontal plane, collision optics)

Left-hand side odd-type low-β triplet, horizontal β : $\sum(KL)_{q_L}\beta(s_{q_L}) = 158.4$
Right-hand side odd-type low-β triplet, horizontal β : $\sum(KL)_{q_R}\beta(s_{q_R}) = 211.6$
Sum and difference of the above yield :
$\sum(KL)_q\beta(s_q) = 370, \quad |\sum(KL)_{q_L}\beta(s_{q_L}) - \sum(KL)_{q_R}\beta(s_{q_R})| = 53$

Sums relative to section 3.2 of the text (crossing scheme, horizontal plane, collision optics)

Left-hand side even-type low-β triplet : $\sum(KL)_{q_L}\beta(s_{q_L}) = 202$
Right-hand side even-type low-β triplet : $\sum(KL)_{q_R}\beta(s_{q_R}) = 146$
Sum and difference of the above give :
$\sum(KL)_q\beta(s_q) = 350, |\sum(KL)_{q_L}\beta(s_{q_L}) - \sum(KL)_{q_R}\beta(s_{q_R})| = 56$

C Appendix : Simplified expressions for the anomalous dispersion

along the LHC ring

The contribution of the low-β triplet pair associated with the non-zero c.o., to the perturbative closed dispersion $d_y(s)$ is split into contributions $d_y^L(s)$ and $d_y^R(s)$ of respectively the left- and right-hand side triplets. This leads to splitting the term $\sum K(s)y_{co}(s)\delta(s-s_q)ds_q$ of Eq. (7) into two separate integrals, for respectively the left and right triplet. The superposition principle thus allows to solve the equation for each triplet independently.

The contribution of the left triplet writes, in the crossing scheme ($y^* = 0$) [after Eq. (10)]

$$d_y^L(s) = y'^*\sqrt{\beta(s)\beta^*}/(2\sin\pi\nu)\sum(KL)_{q_L}\beta(s_{q_L})\sin\nu[\phi(s_{q_L})-\phi^*]\cos\nu[\pi-|\phi(s)-\phi(s_{q_L})|] \quad (48)$$

The index q_L designates the left triplet quadrupoles, the superscript * designates parameters taken

at the IP. Now we assume $\nu[\phi(s_{q_L}) - \phi^*] = -\pi/2$ (this is true at better than 2% within the triplet). It leads to the following simplifications, valid as long as $\sin\nu[\pi - |\phi(s) - \phi^*|]$ is not to small,

$$\begin{aligned}
\cos\nu[\pi - |\phi(s) - \phi(s_{q_L})|] &= \cos\nu[\pi + \phi(s) - \phi(s_{q_L})] = \cos\nu[\pi + \phi(s) - \phi^* - \phi(s_{q_L}) - \phi^*)] \\
&= \cos\nu[\pi + \phi(s) - \phi^*]\cos\nu[\phi(s_{q_L}) - \phi^*] + \sin\nu[\pi + \phi(s) - \phi^*]\sin\nu[\phi(s_{q_L}) - \phi^*] \\
&= -\sin\nu[\pi + \phi(s) - (^*] if \phi(s) < \phi(s_{q_L}) \forall q_L
\end{aligned}$$

$$\begin{aligned}
\cos\nu[\pi &- |\phi(s) - \phi(s_{q_L})|] = \cos\nu[\pi - \phi(s) + \phi(s_{q_L})] = \cos\nu[\pi - \phi(s) + \phi^* + \phi(s_{q_L}) - (^*] \\
&= \cos\nu[\pi - \phi(s) + (^*]\cos\nu[\phi(s_{q_L}) - \phi^*] - \sin\nu[\pi - \phi(s) + (^*]\sin\nu[\phi(s_{q_L}) - \phi^*] \\
&= \sin\nu[\pi - \phi(s) + \phi^*] if \phi(s) > \phi(s_{q_L}) \forall q_L \qquad (49)
\end{aligned}$$

The closed dispersion associated with the left triplet therefore simplifies to

$$\begin{aligned}
d_y^L(s < s_{q_L}) &= y'^* \sqrt{\beta(s)\beta^*}/(2\sin\pi\nu)\sin\nu[\pi + \phi(s) - (^*]\sum(KL)_{q_L}\beta(s_{q_L}), \\
d_y^L(s > s_{q_L}) &= -y'^* \sqrt{\beta(s)\beta^*}/(2\sin\pi\nu)\sin\nu[\pi - \phi(s) + \phi^*]\sum(KL)_{q_L}\beta(s_{q_L}) \qquad (50)
\end{aligned}$$

valid as long as $\sin\nu[\pi - |\phi(s) - \phi^*|]$ is not to small. As concerns the right triplet, $\nu[\phi(s_{q_R}) - \phi^*] = \pi/2$; similar calculations give the closed dispersion

$$\begin{aligned}
d_y^R(s < s_{q_R}) &= y'^* \sqrt{\beta(s)\beta^*}/(2\sin\pi\nu)\sin\nu[\pi + \phi(s) - \phi^*]\sum(KL)_{q_R}\beta(s_{q_R}), \\
d_y^R(s > s_{q_R}) &= -y'^* \sqrt{\beta(s)\beta^*}/(2\sin\pi\nu)\sin\nu[\pi - \phi(s) + \phi^*]\sum(KL)_{q_R}\beta(s_{q_R}) \qquad (51)
\end{aligned}$$

The general solution to Eq. (7) beyond the left and right triplets is therefore

$$\begin{aligned}
d_y(s &< s_{q_L}) = d_y^L(s < s_{q_L}) + d_y^R(s < s_{q_R}) \\
&= y'^* \sqrt{\beta(s)\beta^*}/(2\sin\pi\nu)\sin\nu[\pi + \phi(s) - \phi^*][\sum(KL)_{q_L}\beta(s_{q_L}) + \sum(KL)_{q_R}\beta(s_{q_R})] \\
&= y'^* \sqrt{\beta(s)\beta^*}/(2\sin\pi\nu)\sin\nu[\pi + \phi(s) - \phi^*]\sum(KL)_q\beta(s_q) \qquad (52)
\end{aligned}$$

$$\begin{aligned}
d_y(s > s_{q_L}) &= d_y^L(s > s_{q_L}) + d_y^R(s > s_{q_R}) \\
&= -y'^* \sqrt{\beta(s)\beta^*}/(2\sin\pi\nu)\sin\nu[\pi - \phi(s) + \phi^*]\sum(KL)_{q_L}\beta(s_{q_L}) + \sum(KL)_{q_R}\beta(s_{q_R})] \\
&= -y'^* \sqrt{\beta(s)\beta^*}/(2\sin\pi\nu)\sin\nu[\pi - \phi(s) + \phi^*]\sum(KL)_q\beta(s_q) \qquad (53)
\end{aligned}$$

Combining Eqs. (52, 53) and taking into account the c.o. term $-y_{co}(s)$ leads to Eq. (23). It also provides the closed dispersion between the left and right triplets, namely

$$\begin{aligned}
d_y(s_{q_L} &< s < s_{q_R}) = d_y^L(s > s_{q_L}) + d_y^R(s < s_{q_R}) \\
&= y'^* \sqrt{\beta(s)\beta^*}/(2\sin\pi\nu)\{-\sin\nu[\pi - \phi(s) + \phi^*]\sum(KL)_{q_L}\beta(s_{q_L}) \\
&\qquad + \sin\nu[\pi + \phi(s) - \phi^*]\sum(KL)_{q_R}\beta(s_{q_R})\} \\
&= y'^* \sqrt{\beta(s)\beta^*}/2\{\cos\nu[\phi(s) - \phi^*]\sum\epsilon_q(KL)_q\beta(s_q) \\
&\qquad + \sin([\phi(s) - \phi^*]/\tan\pi\nu\sum(KL)_q\beta(s_q)\} \\
&\qquad [\epsilon_q = \pm 1 \; for \; resp. \; \phi(s) \lessgtr \phi(s_q), \forall q] \qquad (54)
\end{aligned}$$

D Appendix : MAD simulations

- LHC V4.2 optics -

D.1 Single x-crossing/z-off-centering at $IP5$. Optical parameters in the vicinity of the IP's

The following table extracted from a MAD print file displays the betatron functions, phases, and other parameters relevant with the numerical calculations performed in section 3.1 of the text. It includes a $10^{-4} rad$ horizontal closed orbit angle and $10^{-3} m$ vertical closed orbit off-centering at $IP5$ for comparison with the numerical results for the anomalous dispersion provided in sections 3 and 4 of the text.

Table 12: Optical parameters, LHC V4.2 optics. Including $x'^{*} = 10^{-4} rad$ and $z^{*} = 10^{-3} m$ at $IP5$.

ELEMENT SEQUENCE				I	HORIZONTAL						I	VERTICAL				
pos. no.	element name	occ. no.	dist [m]	I	betax [m]	alfax [1]	mux [2pi]	x(co) [mm]	px(co) [.001]	Dx [m]	Dpx [1]	I	betay [m]	alfay [1]	muy [2pi]	y(co) [mm]	py(co) [.001]	Dy [m]	Dpy [1]
1	IP1	1	0.000		0.500	0.000	0.000	0.000	0.000	0.000	-0.024		0.500	0.001	0.000	0.000	0.000	0.000	0.003
3	Q1.R1	1	28.500		2079.668	*******	0.247	0.000	0.000	-0.774	-0.059		1243.313	15.691	0.247	0.000	0.000	0.070	-0.001
5	QT.Q1.R1	1	30.300		2704.737	*******	0.247	0.000	0.000	-0.882	-0.063		1178.228	21.399	0.248	0.000	0.000	0.068	-0.001
7	Q2A.R1	1	36.500		4378.477	-26.180	0.248	0.000	0.000	-1.123	-0.007		1253.042	-41.971	0.249	0.000	0.000	0.071	0.002
9	Q2B.R1	1	43.000		3490.785	180.182	0.248	0.000	0.000	-1.003	0.052		2395.576	*******	0.249	0.000	0.000	0.098	0.007
11	Q3.R1	1	50.800		1790.136	24.775	0.248	0.000	0.000	-0.718	0.010		4428.776	-2.415	0.250	0.000	0.000	0.133	0.000
587	QT.Q3.L2	1	3283.258		1585.815	-22.014	8.736	0.000	0.000	0.674	0.009		4017.383	0.361	7.290	0.000	0.000	0.123	0.000
589	Q3.L2	1	3289.058		2442.825	*******	8.737	0.000	0.000	0.836	0.050		2910.673	179.988	7.290	0.000	0.000	0.105	-0.007
591	Q2B.L2	1	3296.858		4019.274	27.307	8.737	0.000	0.000	1.073	-0.007		1169.991	39.833	7.291	0.000	0.000	0.067	-0.002
593	Q2A.L2	1	3303.358		2639.600	188.882	8.737	0.000	0.000	0.870	-0.062		989.862	-18.123	7.292	0.000	0.000	0.061	0.001
595	QT.Q1.L2	1	3305.558		1894.746	146.376	8.738	0.000	0.000	0.737	-0.057		1060.517	-11.622	7.292	0.000	0.000	0.063	0.001
597	Q1.L2	1	3311.358		882.531	42.001	8.738	0.000	0.000	0.503	-0.024		881.601	41.960	7.293	0.000	0.000	0.058	-0.003
599	IP2	1	3332.358		0.500	0.000	8.985	0.000	0.000	0.001	-0.024		0.500	-0.003	7.540	0.000	0.000	0.000	-0.003
601	Q1.R2	1	3358.858		1068.593	11.675	9.232	0.000	0.000	-0.551	0.006		1806.485	*******	7.786	0.000	0.000	-0.083	-0.007
603	QT.Q1.R2	1	3360.658		1016.426	18.377	9.232	0.000	0.000	-0.538	0.010		2379.860	*******	7.786	0.000	0.000	-0.095	-0.007
605	Q2A.R2	1	3366.858		1092.748	-38.511	9.233	0.000	0.000	-0.558	-0.020		3961.593	-27.096	7.787	0.000	0.000	-0.123	-0.001
607	Q2B.R2	1	3373.358		2143.642	*******	9.234	0.000	0.000	-0.782	-0.056		3160.901	166.651	7.787	0.000	0.000	-0.110	0.006
609	Q3.R2	1	3381.158		4020.929	-0.358	9.234	0.000	0.000	-1.071	0.000		1597.689	22.089	7.788	0.000	0.000	-0.078	0.001
2398	QT.Q3.L51	1	13278.332		4431.270	2.415	31.391	-4.707	0.003	-0.707	0.001		1767.406	-24.562	31.407	0.614	0.042	0.048	0.001
2400	Q3.L5	1	13284.132		3227.889	194.256	31.391	-4.017	0.242	-0.603	0.036		2699.084	*******	31.407	0.964	0.084	0.058	0.003
2402	Q2B.L5	1	13291.932		1338.724	43.387	31.392	-2.587	0.084	-0.388	0.013		4411.264	26.220	31.408	1.428	0.013	0.074	0.000
2404	Q2A.L5	1	13298.432		1148.763	-21.133	31.392	-2.396	-0.044	-0.359	-0.006		2968.115	201.521	31.408	1.301	-0.062	0.061	-0.004
2406	QT.Q1.L51	1	13300.632		1234.248	-15.637	31.393	-2.484	-0.031	-0.372	-0.005		2165.561	160.378	31.408	1.168	-0.056	0.052	-0.004
2408	Q1.L5	1	13306.432		1058.461	45.998	31.393	-2.300	0.100	-0.343	0.015		1053.826	45.797	31.409	1.000	0.000	0.037	-0.002
2410	IP5	1	13329.432		0.500	0.000	31.640	0.000	0.100	0.001	0.015		0.502	-0.001	31.655	1.000	0.000	0.001	-0.002
2412	Q1.R5	1	13357.932		2079.493	*******	31.887	3.224	0.244	0.485	0.037		1238.261	15.629	31.902	0.856	-0.051	-0.037	0.000
2414	QT.Q1.R51	1	13359.732		2704.511	*******	31.887	3.677	0.262	0.552	0.039		1173.433	21.314	31.903	0.761	-0.055	-0.036	0.001
2416	Q2A.R5	1	13365.932		4378.110	-26.178	31.888	4.678	0.028	0.702	0.004		1247.916	-41.797	31.903	0.514	-0.023	-0.038	-0.001
2418	Q2B.R5	1	13372.432		3490.494	180.167	31.888	4.177	-0.216	0.628	-0.032		2385.740	*******	31.904	0.434	0.001	-0.052	-0.004
2420	Q3.R5	1	13380.232		1789.987	24.773	31.888	2.992	-0.041	0.453	-0.006		4410.555	-2.403	31.904	0.382	-0.021	-0.071	0.000
4186	QT.Q3.L81	1	23277.406		1585.812	-22.013	55.496	0.000	0.000	-0.662	-0.009		4019.471	0.355	54.073	0.000	0.000	-0.126	0.000
4188	Q3.L8	1	23283.206		2442.820	*******	55.497	0.000	0.000	-0.822	-0.049		2912.245	180.079	54.073	0.000	0.000	-0.108	0.007
4190	Q2B.L8	1	23291.006		4019.266	27.307	55.497	0.000	0.000	-1.054	0.007		1170.690	39.851	54.074	0.000	0.000	-0.068	0.002
4192	Q2A.L8	1	23297.506		2639.594	188.882	55.497	0.000	0.000	-0.855	0.061		990.533	-18.141	54.075	0.000	0.000	-0.063	-0.001
4194	QT.Q1.L81	1	23299.706		1894.743	146.376	55.498	0.000	0.000	-0.724	0.056		1061.263	-11.636	54.075	0.000	0.000	-0.065	-0.001
4196	Q1.L8	1	23305.506		882.530	42.001	55.498	0.000	0.000	-0.495	0.023		882.284	41.986	54.076	0.000	0.000	-0.059	0.003
4198	IP8	1	23326.506		0.500	0.000	55.745	0.000	0.000	-0.003	0.023		0.500	0.003	54.322	0.000	0.000	0.000	0.003
4200	Q1.R8	1	23353.006		1068.589	11.675	55.992	0.000	0.000	0.540	-0.006		1806.912	*******	54.569	0.000	0.000	0.085	0.007
4202	QT.Q1.R81	1	23354.806		1016.422	18.377	55.992	0.000	0.000	0.526	-0.009		2380.450	*******	54.569	0.000	0.000	0.097	0.007
4204	Q2A.R8	1	23361.006		1092.745	-38.511	55.993	0.000	0.000	0.547	0.019		3962.668	-27.110	54.570	0.000	0.000	0.126	0.001
4206	Q2B.R8	1	23367.506		2143.636	*******	55.994	0.000	0.000	0.766	0.055		3161.827	166.694	54.570	0.000	0.000	0.112	-0.00
4208	Q3.R8	1	23375.306		4020.918	-0.358	55.994	0.000	0.000	1.050	0.000		1598.232	22.091	54.570	0.000	0.000	0.080	-0.001
4784	QT.Q3.L11	1	26607.764		4431.634	2.415	63.031	0.000	0.000	1.130	-0.001		1774.800	-24.666	63.062	0.000	0.000	-0.084	-0.001
4786	Q3.L1	1	26613.564		3228.154	194.272	63.031	0.000	0.000	0.964	-0.058		2710.402	*******	63.062	0.000	0.000	-0.104	-0.006
4788	Q2B.L1	1	26621.364		1338.834	43.390	63.032	0.000	0.000	0.621	-0.020		4429.794	26.328	63.063	0.000	0.000	-0.133	0.001
4790	Q2A.L1	1	26627.864		1148.857	-21.135	63.032	0.000	0.000	0.575	0.011		2980.600	202.367	63.063	0.000	0.000	-0.109	0.007
4792	QT.Q1.L11	1	26630.064		1234.348	-15.638	63.033	0.000	0.000	0.596	0.008		2174.676	161.051	63.063	0.000	0.000	-0.093	0.007
4794	Q1.L1	1	26635.864		1058.546	46.002	63.033	0.000	0.000	0.552	-0.024		1058.276	45.989	63.064	0.000	0.000	-0.065	0.003
4796	IP1.L1	1	26658.864		0.500	0.000	63.280	0.000	0.000	0.000	-0.024		0.500	0.001	63.310	0.000	0.000	0.000	0.003

D.2 Multiple crossing, at $IP1, 2, 5$ and 8. Optical parameters in the vicinity of the IP's

The following table extracted from a MAD print file displays the betatron functions, phases, and other parameter relevant with the numerical calculations performed in section 3.2 of the report. It includes horizontal c.o. angles $x'^* = 10^{-4} rad$ at $IP1/2$ and $-10^{-4} rad$ at $IP5/8$, as well as vertical closed orbit angles $z'^* = 10^{-4} rad$ at $IP1$ and $-10^{-4} rad$ at $IP5$, for comparison with the numerical results provided in sections 3.2 and 4.

Table 13: Optical parameters, LHC V4.2 optics. Including $x'^* = 10^{-4} rad$ at $IP1/2$ and $-10^{-4} rad$ at $IP5/8$, together with $z'^* = 10^{-4} rad$ at $IP1$ and $-10^{-4} rad$ at $IP5$.

ELEMENT SEQUENCE				I	HORIZONTAL						I	VERTICAL					
pos. no.	element name	occ. no.	dist [m]	I	betax [m]	alfax [1]	mux [2pi]	x(co) [mm]	px(co) [.001]	Dx [m]	Dpx [1]	I	betay [m]	alfay [1]	muy [2pi]	y(co) [mm]	py(co) [.001]	DY [m]	Dpy [1]
1	IP1	1	0.000		0.500	0.000	0.000	0.000	0.100	0.004	0.070		0.500	0.001	0.000	0.000	0.100	-0.001	0.035
3	Q1.R1	1	28.500		2079.664	*******	0.247	3.224	0.244	2.246	0.170		1243.315	15.691	0.247	2.493	-0.031	0.861	-0.011
5	QT.Q1.R1	1	30.300		2704.732	*******	0.247	3.677	0.262	2.561	0.183		1178.229	21.399	0.248	2.427	-0.044	0.839	-0.015
7	Q2A.R1	1	36.500		4378.469	-26.180	0.248	4.678	0.028	3.258	0.020		1253.043	-41.971	0.249	2.503	0.084	0.866	0.029
9	Q2B.R1	1	43.000		3490.779	180.181	0.248	4.177	-0.216	2.910	-0.150		2395.578	*******	0.249	3.461	0.242	1.197	0.084
11	Q3.R1	1	50.800		1790.133	24.775	0.248	2.992	-0.041	2.086	-0.029		4428.780	-2.415	0.250	4.706	0.003	1.628	0.001
601	QT.Q3.L2	1	3283.258		1585.812	-22.013	8.736	-2.816	-0.039	-1.927	-0.027		4017.384	0.361	7.290	0.000	0.000	1.717	0.000
603	Q3.L2	1	3289.058		2442.821	*******	8.737	-3.494	-0.210	-2.394	-0.144		2910.674	179.989	7.290	0.000	0.000	1.462	-0.090
605	Q2B.L2	1	3296.858		4019.267	27.307	8.737	-4.482	0.030	-3.072	0.021		1169.992	39.833	7.291	0.000	0.000	0.928	-0.031
607	Q2A.L2	1	3303.358		2639.595	188.882	8.737	-3.632	0.260	-2.492	0.178		989.863	-18.123	7.292	0.000	0.000	0.855	0.016
609	QT.Q1.L2	1	3305.558		1894.743	146.376	8.738	-3.077	0.238	-2.113	0.163		1060.517	-11.622	7.292	0.000	0.000	0.885	0.010
611	Q1.L2	1	3311.358		882.530	42.001	8.738	-2.100	0.100	-1.446	0.068		881.602	41.960	7.293	0.000	0.000	0.808	-0.038
613	IP2	1	3332.358		0.500	0.000	8.985	0.000	0.100	-0.020	0.068		0.500	-0.003	7.540	0.000	0.000	0.005	-0.03
615	Q1.R2	1	3358.858		1068.591	11.675	9.232	2.311	-0.025	1.552	-0.016		1806.486	*******	7.786	0.000	0.000	-1.145	-0.091
617	QT.Q1.R2	1	3360.658		1016.424	18.377	9.232	2.254	-0.041	1.516	-0.026		2379.861	*******	7.786	0.000	0.000	-1.314	-0.099
619	Q2A.R2	1	3366.858		1092.746	-38.511	9.233	2.337	0.082	1.578	0.057		3961.595	-27.096	7.787	0.000	0.000	-1.697	-0.012
621	Q2B.R2	1	3373.358		2143.638	*******	9.234	3.274	0.236	2.216	0.161		3160.902	166.652	7.787	0.000	0.000	-1.516	0.080
623	Q3.R2	1	3381.158		4020.921	-0.358	9.234	4.484	0.000	3.039	0.001		1597.689	22.089	7.788	0.000	0.000	-1.079	0.015
2418	QT.Q3.L51	1	13278.332		4431.277	2.415	31.391	4.707	-0.003	3.930	-0.002		1767.405	-24.562	31.407	2.979	0.041	1.033	0.014
2420	Q3.L5	1	13284.132		3227.893	194.256	31.391	4.017	-0.242	3.354	-0.202		2699.082	*******	31.407	3.681	0.216	1.274	0.074
2422	Q2B.L5	1	13291.932		1338.726	43.387	31.392	2.587	-0.084	2.159	-0.070		4411.261	26.220	31.408	4.706	-0.028	1.626	-0.010
2424	Q2A.L5	1	13298.432		1148.765	-21.133	31.392	2.396	0.044	1.998	0.036		2968.113	201.521	31.408	3.860	-0.262	1.334	-0.091
2426	QT.Q1.L51	1	13300.632		1234.250	-15.637	31.393	2.484	0.031	2.070	0.026		2165.559	160.378	31.408	3.297	-0.244	1.140	-0.084
2428	Q1.L5	1	13306.432		1058.462	45.998	31.393	2.300	-0.100	1.916	-0.084		1053.825	45.797	31.409	2.300	-0.100	0.795	-0.035
2430	IP5	1	13329.432		0.500	0.000	31.640	0.000	-0.100	-0.005	-0.084		0.502	-0.001	31.655	0.000	-0.100	0.001	-0.035
2432	Q1.R5	1	13357.932		2079.497	*******	31.887	-3.224	-0.244	-2.697	-0.204		1238.260	15.629	31.902	-2.493	0.031	-0.860	0.011
2434	QT.Q1.R51	1	13359.732		2704.515	*******	31.887	-3.677	-0.262	-3.076	-0.219		1173.432	21.314	31.903	-2.427	0.044	-0.837	0.015
2436	Q2A.R5	1	13365.932		4378.117	-26.178	31.888	-4.678	-0.028	-3.913	-0.023		1247.915	-41.797	31.903	-2.503	-0.084	-0.865	-0.029
2438	Q2B.R5	1	13372.432		3490.499	180.167	31.888	-4.177	0.216	-3.494	0.180		2385.738	*******	31.904	-3.461	-0.242	-1.196	-0.0
2440	Q3.R5	1	13380.232		1789.990	24.773	31.888	-2.992	0.041	-2.504	0.034		4410.552	-2.403	31.904	-4.706	-0.003	-1.626	-0.001
4214	QT.Q3.L81	1	23277.406		1585.809	-22.013	55.496	2.816	0.039	2.052	0.028		4019.475	0.355	54.073	0.000	0.000	-1.501	0.000
4216	Q3.L8	1	23283.206		2442.816	*******	55.497	3.494	0.210	2.542	0.152		2912.247	180.080	54.073	0.000	0.000	-1.276	0.079
4218	Q2B.L8	1	23291.006		4019.258	27.307	55.497	4.482	-0.030	3.256	-0.023		1170.691	39.851	54.074	0.000	0.000	-0.807	0.028
4220	Q2A.L8	1	23297.506		2639.590	188.882	55.497	3.632	-0.260	2.637	-0.189		990.534	-18.141	54.075	0.000	0.000	-0.739	-0.013
4222	QT.Q1.L81	1	23299.706		1894.739	146.376	55.498	3.077	-0.238	2.233	-0.173		1061.264	-11.636	54.075	0.000	0.000	-0.764	-0.008
4224	Q1.L8	1	23305.506		882.528	42.001	55.498	2.100	-0.100	1.522	-0.073		882.285	41.986	54.076	0.000	0.000	-0.694	0.034
4226	IP8	1	23326.506		0.500	0.000	55.745	0.000	-0.100	-0.011	-0.073		0.500	0.003	54.322	0.000	0.000	0.010	0.034
4228	Q1.R8	1	23353.006		1068.587	11.675	55.992	-2.311	0.025	-1.697	0.019		1806.914	*******	54.569	0.000	0.000	1.020	0.080
4230	QT.Q1.R81	1	23354.806		1016.421	18.377	55.992	-2.254	0.041	-1.654	0.030		2380.452	*******	54.569	0.000	0.000	1.170	0.088
4232	Q2A.R8	1	23361.006		1092.743	-38.511	55.993	-2.337	-0.082	-1.713	-0.060		3962.672	-27.110	54.570	0.000	0.000	1.508	0.010
4234	Q2B.R8	1	23367.506		2143.632	*******	55.994	-3.274	-0.236	-2.396	-0.172		3161.829	166.694	54.570	0.000	0.000	1.346	-0.071
4236	Q3.R8	1	23375.306		4020.910	-0.358	55.994	-4.484	0.000	-3.279	0.000		1598.233	22.091	54.570	0.000	0.000	0.955	-0.014
4826	QT.Q3.L11	1	26607.764		4431.627	2.415	63.031	-4.707	0.003	-3.274	0.002		1774.802	-24.666	63.062	-2.979	-0.041	-1.034	-0.014
4828	Q3.L1	1	26613.564		3228.148	194.272	63.031	-4.017	0.242	-2.793	0.168		2710.404	*******	63.062	-3.681	-0.216	-1.276	-0.075
4830	Q2B.L1	1	26621.364		1338.831	43.390	63.032	-2.587	0.084	-1.799	0.059		4429.798	26.328	63.063	-4.706	0.028	-1.628	0.010
4832	Q2A.L1	1	26627.864		1148.855	-21.135	63.032	-2.396	-0.044	-1.664	-0.030		2980.602	202.368	63.063	-3.860	0.262	-1.336	0.091
4834	QT.Q1.L11	1	26630.064		1234.346	-15.638	63.033	-2.484	-0.031	-1.725	-0.022		2174.678	161.051	63.063	-3.297	0.244	-1.141	0.085
4836	Q1.L1	1	26635.864		1058.544	46.002	63.033	-2.300	0.100	-1.596	0.070		1058.277	45.989	63.064	-2.300	0.100	-0.797	0.035
4838	IP1.L1	1	26658.864		0.500	0.000	63.280	0.000	0.100	0.004	0.070		0.500	0.001	63.310	0.000	0.100	-0.001	0.035

E Appendix : MAD match file

used in the tuning of the LHC 4.2 Interaction Regions

The following MAD match file is used for re-tuning the IR in the case of Self-absorption within regular IR tuning procedures, section 5.1 of the text. The values of constraints and weights are as in Ref.[16].

```
! LHC V4 odd insertion matching
SIR1MATCH: SUBROUTINE

TWISS, beta0 = sir5, mux = 0.0, muy = 0.0
MATCH, beta0 = sir5, mux = 0.0, muy = 0.0, orbit
VARY, KQ1.L5,     STEP=1.0E-07, UPPER=  KMAX, LOWER= -KMAX
VARY, KQT1.L5,  STEP=1.0E-07, UPPER=  KMAX, LOWER= -KMAX
VARY, KQT3.L5,  STEP=1.0E-07, UPPER=  KMAX, LOWER= -KMAX
VARY, KQ4.L5,     STEP=1.0E-07, UPPER=  KMAX, LOWER= -KMAX
VARY, KQ5.L5,     STEP=1.0E-07, UPPER=  KMAX, LOWER= -KMAX
VARY, KQ6.L5,     STEP=1.0E-07, UPPER=  KMAX, LOWER= -KMAX
VARY, KQT7.L5,   STEP=1.0E-07, UPPER=  KMAX, LOWER= -KMAX
VARY, KQT8.L5,   STEP=1.0E-07, UPPER=  KMAX, LOWER= -KMAX
VARY, KQT9.L5,   STEP=1.0E-07, UPPER=  KMAX, LOWER= -KMAX
VARY, KQT10.L5, STEP=1.0E-07, UPPER=  KMAX, LOWER= -KMAX
VARY, BMAX5 ,STEP=1.0E-02, UPPER= 5000, LOWER=  200
WEIGHT,     BETX = 100,     ALFX = 10,     DX = 10,    DPX = 100
CONSTRAINT, PLACE= $IP5$,                                          >
            BETX = BSTAR,   ALFX = 0.0,    DX = 0.0,   DPX = 0.
WEIGHT,     BETX = 1,       ALFX = 10,     DX = 10,    DPX = 100,       >
            BETY = .0,      ALFY = 0.,     DY =  0,    DPY =   0,      >
           MUY =  0,       X = 0, Y = 0,  PX = 0, PY = 0,   MUX=1.00
CONSTRAINT, PLACE= E.IR5,  >
            BETA0 = EIR5, MUX=SMU5
CONSTRAINT, PLACE = qt.q3.15,    BETX = BMAX5
CONSTRAINT, PLACE = q2r5    ,    BETX = BMAX5

LMDIF, CALLS =  1000, TOLERANCE = 1.0E-12
ENDMATCH
ENDSUBROUTINE
RETURN;
```

References

[1] The Large Hadron Collider, Conceptual Design, CERN/AC/95-05 (LHC), CERN, 20 Oct. 1995.

[2] W. Herr, Is there an alternative to alternating crossing scheme in LHC ?, CERN/SL/93-45 (AP) LHCNote 258, CERN, Nov. 1993, and, W. Herr, Tune shifts and spreads due to the long range beam-beam effects in the LHC, CERN/SL/90-06 (AP) and LHC Note 119 (1990).

[3] J. Miles, Beam-beam effects, in Proc. LHC Machine Advisory Committee, Nov. 6, 1996, CERN.

[4] H. Grote, F. C. Iselin, The MAD Program, User's Reference Manual, CERN/SL/90-13 (AP), CERN, 19 Jan. 1995.

[5] T. Risselada, CERN/SL/AP, provided the MAD files for LHC Version 4.2, namely : lhc42.K-collision, lhc42.K-injection, lhc42.sequence.

[6] K.L. Brown, First and second order charged particle optics, Proc. AIP Conf. No 127, Ed. M. Month, N.Y. 1985.

[7] G. Leleux, Compléments sur la physique des accélérateurs, D.E.A. de Physique et Technologie des Grands Instruments, Université Paris VI, Rapport CEA-Saclay/LNS/86-101, Mars 1986.

[8] After discussion with S.Y. Lee, FNAL, January 1997.

[9] T. Risselada, Gamma transition jump schemes, CERN Accelerator School, Finland, Report CERN 94-01, 26 Jan. 1994, Vol. 1.

[10] A. Faus-Golfe, J. P. Koutchouk, A. Verdier, Analysis and improvement of the dispersion matching in LHC, LHC Project Note 32, CERN, Feb. 26, 1996

[11] W. Herr, Luminosity limitations in the LHC due to beam-beam effects for different bunch spacing, CERN SL/Note 92-51 (AP), CERN, 21 Sept. 1992.

[12] J. Jowett, RDTWISS computer code, private communication, CERN, 1994.

[13] A. Faus-Golfe and A. Verdier, Dynamic aperture limitations of the LHC in physics conditions due to low-β insertions, Proc. EPAC Conf. 1996.

[14] Y. Nosochkov, D. M. Ritson, The provision of IP crossing angles for the SSC, IEEE Trans. 1993.

[15] A. Verdier, Operational Q-shifts and b2 compensation in LHC, LHC Project Note 26, CERN, 8 Jan. 1996.

[16] X. Luo, F. Méot, W. Scandale, The LHC lattice, Version 3, SL/Note 94-28 (AP), CERN, 1994, and A. Garren, X. Luo, F. Méot, W. Scandale, The LHC lattice, Version 4, SL/Note 95-06 (AP) and LHC Note 314, CERN, 1995.

[17] Proc. LHC Machine Advisory Committee, Nov. 6, 1996, CERN.